Dynamic Magnetic Resonance Imaging of Tumor Perfusion

Approaches and Biomedical Challenges

BY DAVID J. COLLINS AND ANWAR R. PADHANI

Dynamic contrast enhanced magnetic resonance imaging (DCE-MRI) using small molecular weight gadolinium chelates enables noninvasive imaging characterization of tissue vascularity. Depending on the technique used, data reflecting tissue perfusion (blood flow, blood volume, mean transit time), microvessel permeability surface area product, and extracellular leakage space can be obtained. Insights into these physiological processes can be obtained from inspection of kinetic enhancement curves or by the application of complex compartmental modeling techniques. Potential clinical applications include screening for malignant disease, lesion characterization, monitoring lesion response to treatment, and assessment of residual disease. Newer applications include prognostication, pharmacodynamic assessments of antivascular anticancer drugs, and predicting efficacy of treatment. For dynamic MRI to enter into widespread clinical practice, it will be necessary to develop standardized approaches to measurement and robust analysis approaches. These include the need for commercial equipment manufacturers to provide robust methods for rapidly measuring time-varying change in T1 relaxation rates, incorporation of arterial input function into kinetic modeling processes, robust analysis software that allows input from a variety of MRI devices, and validated statistical tools for the evaluation of heterogeneity.

Introduction

Angiogenesis, the sprouting of new capillaries from existing blood vessels and vasculogenesis, the de novo generation of blood vessels are the two primary methods of vascular expansion by which nutrient supply to tissues is adjusted to match physiological needs. Angiogenesis is an essential component of several normal physiological processes, including menstrual cycle changes in the ovaries and uterus, organ regeneration, wound healing, and the spontaneous growth of collateral vessels in response to ischemia [1]. Pathological angiogenesis is an integral part of a number of disease states, including rheumatoid disease, age-related macular degeneration, proliferative retinopathy, and psoriasis, as well as being critical for growth and metastasis of malignant tumors [2].

There are a number of distinguishing features that are characteristic of malignant vasculature, many of which are amenable to study by MRI methods [3]. These include:

- Spatial heterogeneity and chaotic structure—little hierarchy of vascular structures is observed with abrupt changes in diameter and blind ending vessels, particularly within the centers of tumors; few structurally complete arteries or veins are found with sinusoidal capillary plexuses prevailing. The remodeling of the vasculature seen in inflammation or wound healing is largely missing.
- Poorly formed, fragile vessels with high permeability to macromolecules, due to the presence of large endothelial cell gaps or fenestrae [4], incomplete basement membrane and relative lack of pericytes or smooth muscle associations with endothelial cells [5].
- Arteriovenous shunting, high vascular tortuosity and vasodilatation [6].
- Intermittent or unstable blood flow (with acutely collapsing vessels) [7] and areas of spontaneous hemorrhage.
- Extreme heterogeneity of vascular density with areas of low vascular density mixed with regions of high angiogenic activity [6].

Biological and Clinical Importance of Tumor Angiogenesis

Tumor growth beyond 1–2 mm in solid tissues cannot occur without vascular support [8]. Transgenic animal tumor model experiments have shown that progression from an in situ to invasive cancer is accompanied by the onset of angiogenesis [9]. There are a number of clinical examples where vascularization has been related to tumor progression (e.g., in the change from breast ductal carcinoma in situ to invasive cancer [10] and in the transformation of dysplastic nodules to hepatocelluar carcinoma [11]). Patient prognosis is related to the state of tumor angiogenesis; elevated tumor levels of the proangiogenic cytokine vascular endothelial growth factor (VEGF) is associated with poorer overall prognosis in breast cancer [12]–[14]. Immunohistochemical measurement of angiogenic activity by microvessel density estimations has been shown to be an important prognostic factor for overall survival that is independent of other known prognostic variables, including stage, histological grade, and lymph node involvement in a number of cancer types [15]. Additionally, vascular access is essential for a tumor to be able to metastasize to distant sites [9].

0739-5175/04/$20.00©2004IEEE

For dynamic MRI to enter into widespread clinical practice, it will be necessary to develop standardized approaches to measurement and robust analysis approaches.

Methods for Assessing Tissue Vascularity

Current methods of assessing angiogenesis can be considered as either direct or indirect. The most frequently used direct method is microvessel density (MVD) counting after the immunostaining with a variety of panendothelial antibodies that include factor VIII related antigen, CD34 and CD31 [16]. This technique requires tumor tissue generally from operative specimens and is unable to inform on the functional state of the vasculature. More recently, indirect, or surrogate, methods of assessing angiogenesis, such as blood levels of angiogenic factors (VEGF), fibroblastic growth factor (FGF) [17], and imaging methods have been used. Advantages of indirect methods are that they are noninvasive, can be performed with the tumor in situ, and may be used to monitor response to treatment. Indirect techniques are quantitative and, in the case of imaging, the functional status of the vasculature can be assessed. It is important to note that implanted tumor xenograft data show that there is a discrepancy between perfused and visible microvessels; a variable 20–85% of microvessels are perfused at any given time. This results in a difference between histological MVD and what is described as the "true or functional vascular density" [18].

Imaging Tissue Vascularity with MRI

Potentially, imaging assessments of the functional tumor vasculature could have widespread clinical applications; recently, developments in angiogenesis imaging have gained greater impetus by the development of anticancer drugs that target the functioning tumor microvasculature [19]. The need for imaging biomarkers that inform on drug action noninvasively has been widely recognized. Several imaging techniques are able to assess human tumors with respect to their angiogenic status. MRI techniques can be divided into nonenhanced and contrast media enhanced methods [3], [20]–[23]. The latter can be further divided by the type of contrast medium used; (i) low molecular weight agents (<1000 Daltons) that rapidly diffuse in the extracellular fluid space (ECF agents), (ii) large-molecular agents (>30,000 Daltons) designed for prolonged intravascular retention [macromolecular contrast media (MMCM), or blood pool agents] [22], and (iii) agents intended to accumulate at sites of concentrated angiogenesis mediating molecules [24]. Tumor vascularity can also be analyzed using intrinsic blood oxygenation level dependent (BOLD) contrast MRI [25]. This review concentrates exclusively on noninvasive characterization of tumor neovasculature with DCE-MRI using low-molecular weight contrast agents and explains how perfusion-related data can be construed or extracted, depending on the technique used [26]–[28].

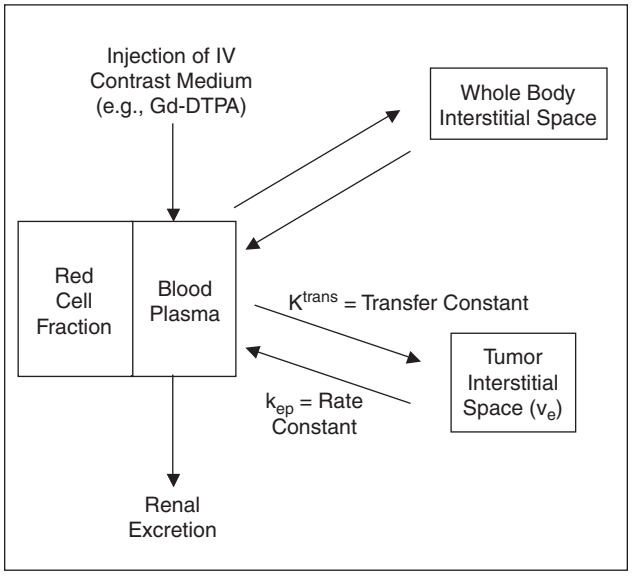

Fig. 1. Body compartments accessed by low molecular weight contrast media injected intravenously.

MRI Contrast Agent Kinetics

DCE-MRI is able to distinguish malignant from benign and normal tissues by exploiting differences in contrast agent behavior in their respective microcirculations. When a bolus of paramagnetic, low molecular weight contrast agent passes through a capillary bed, it is transiently confined within the vascular space. The "first pass" includes the arrival of contrast medium and lasts for a few cardiac cycles. Within the vascular space and in the immediate vicinity, paramagnetic contrast media produces magnetic field (Bo) inhomogeneities that result in a decrease in the signal intensity of surrounding tissues. In most tissues, except the brain, testes, and retina, the contrast agent rapidly passes into the extravascular-extracellular space (EES, also called leakage space—v_e) at a rate determined by the permeability of the microvessels, their surface area, and by blood flow (Figure 1). In tumors, typically 12–45% of the contrast media leaks into the EES during the first pass [29]. The transfer constant (K^{trans}) describes the transendothelial transport of low molecular weight contrast medium. Three major factors determine the behavior of low molecular weight contrast media in tissues during the first few minutes after injection; blood perfusion, transport of contrast agent across vessel walls, and diffusion of contrast medium in the interstitial space. If the delivery of the contrast medium to a tissue is insufficient (flow-limited situations or where vascular permeability is greater than inflow), then blood perfusion will be the dominant factor determining contrast agent kinetics and K^{trans} approximates to tissue blood flow per unit volume [30]. The latter situation is commonly found in tumors. If tissue perfusion is sufficient and transport out of the vasculature does not deplete

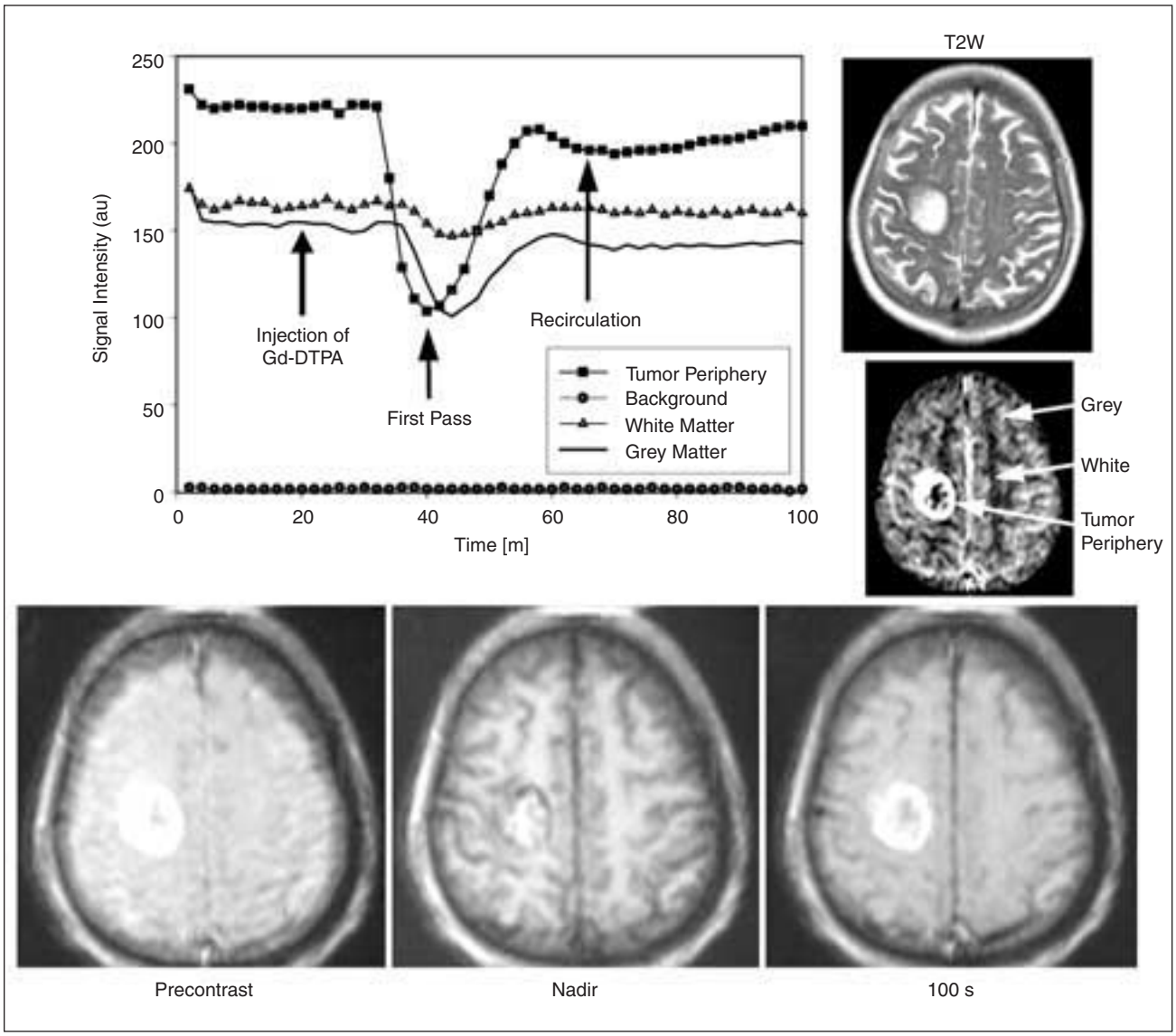

Fig. 2. Typical T2*-weighted DCE-MRI study of a patient with a malignant astrocytoma. 30 ml of IV contrast Gd-DTPA was given after the tenth data point. First-pass T2* susceptibility effects cause marked darkening of the tumor periphery. Darkening of the grey matter of the brain is greater than the less vascular white matter. The first pass and recirculation phases are indicated. Signal intensity changes for four ROIs are shown in the insert (subtraction T2* image of the nadir point for the tumor ROI). An anatomic T2-weighted image at the same slice position is also shown for reference.

intravascular contrast medium concentration (nonflow limited situations), then transport across the vessel wall is the major factor that determines contrast medium kinetics [K^{trans} then approximates to permeability surface area product (PS)]. The latter circumstance occurs in areas of radiation fibrosis, in the presence of an intact blood brain barrier, but can also occur in extracranial tumors, usually after treatment.

As low molecular weight contrast media do not cross cell membranes, the volume of distribution is effectively the EES (v_e). Contrast medium also begins to diffuse into tissue compartments further removed from the vasculature, including areas of necrosis and fibrosis. Over a period typically lasting several minutes to hours, the contrast agent diffuses back into the vasculature (described by the rate constant or k_{ep}) from where it is excreted (usually by the kidneys, although some ECF contrast media have significant hepatic excretion). When capillary permeability is very high, the return of contrast medium is typically rapid, resulting in faster washout as plasma contrast agent concentrations fall. Contrast medium elimination from very slow-exchange tissues, such as fibrosis and necrosis, occurs slowly, explaining the persistent delayed enhancement described in some tumors, such as cholangiocarcinoma and hepatic colorectal metastases.

MRI sequences can be designed to be sensitive to the vascular phase of contrast medium delivery (so-called T2* methods, which reflect on tissue perfusion and blood volume) [31], [32]. T1-weighted sequences are sensitive to the presence of contrast medium in the EES and thus reflect microvessel perfusion, permeability, and extracellular leakage space. These two methods are compared in Table 1. The analysis methods for evaluating these techniques have their foundations in basic physiology and pharmacology [33]–[35].

Table 1. Comparison of T2*- and T1-weighted dynamic contrast enhanced MRi techniques.

	T2*W imaging	T1W imaging
Tissue signal intensity change	Darkening	Enhancement
Duration of effect and optimal data acquisition	Seconds/subsecond	Min/2–25 s
Magnitude of effect	Small	Larger
Optimal contrast medium dose	$\geq$ 0.2 mmol/kg	0.1–0.2 mmol/kg
Quantification method used	Relative more than absolute	Relative and absolute
Physiological property measured	Perfusion/blood volume	Transendothelial permeability, capillary surface area, lesion leakage space
Kinetic parameters derived	Blood volume and flow, transit time	Transfer and rate constants, leakage space
Pathological correlates	Tumor grade and microvessel vessel density	Microvessel density Vascular endothelial growth factor (VEGF)
Clinical MR applications	Lesion characterization—breast, liver and brain	Lesion detection and characterization
	Noninvasive brain tumor grading	Improving accuracy of tumor staging
	Directing brain tumor biopsy	Predicting response to treatment
	Determining brain tumor prognosis	Monitoring response to treatment
	Monitoring treatment e.g. radiotherapy	Novel therapies including antiangiogenic drugs
		Detecting tumor relapse

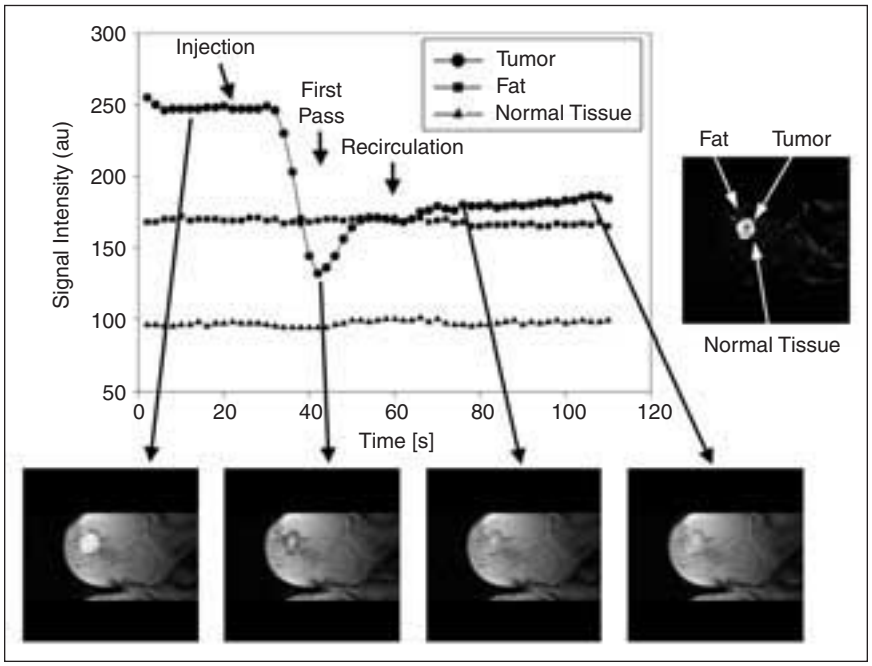

Fig. 3. Typical T2*-weighted DCE-MRI study of a patient with an invasive ductal cancer of the breast. A patient with breast cancer (same patient illustrated in Figures 5, 6, 8, and 10). 22 ml of IV contrast Gd-DTPA was given after the tenth data point. First-pass T2* susceptibility effects cause marked darkening of the tumor with no alteration in signal intensity of fibroglandular breast parenchyma (normal tissue) or fat. The first-pass and recirculation phases can clearly be seen. Insert shows a subtraction T2* image of the nadir point for the tumor ROI.

T2*-Weighted DCE-MRI

Data Acquisition

Perfusion-weighted images can be obtained with bolus-tracking techniques that monitor the passage of contrast material through a capillary bed [31], [32]. A decrease in signal intensity of tissues occurs due to the presence of concentrated contrast media within vessels and in their immediate vicinity (Figures 2 and 3). Susceptibility-weighted (T2*-weighted) spin-echo sequences are more sensitive to capillary blood flow compared with gradient-echo sequences, which incorporate signals from larger vessels [36]. The degree of signal intensity loss is dependent on the vascular concentration of the contrast agent and microvessel size [37] and density. The signal to noise ratio (SNR) of T2*-weighted DCE-MRIs can be improved by using high doses of contrast medium (i.e., $\geq$ 0.2-mmol/kg body weight) [38]. Standard spoiled gradient-echo sequences on conventional MRI systems can characterize these effects but are limited to a few slices. High specification, echo-planar MRI systems capable of rapid

image acquisition allow greater anatomical coverage. However, echo-planar sequences have limited applications in extracranial tissues owing to great intrinsic sensitivity to susceptibility inducing environments (e.g., highly concentrated contrast media and that caused by bowel gas) which can result in spatial misregistration of major vessels during the first passage of the contrast agent thorough the vessels [39].

Quantification

Tracer kinetic principles can be used to provide estimates of relative blood volume (rBV), relative blood flow (rBF) and mean transit time (MTT) derived from the first-pass of contrast agent through the microcirculation [31], [32], [40] (Figure 4). MTT is the average time the contrast agent takes to pass through the tissue being studied. These variables are related by the central volume theorem equation (BF = BV/MTT). A number of conditions of the central volume theorem cannot be met in biological tissues. For example, injection time is not instantaneous, and, as the arterial input function is not typically measured, these parameter estimates are usually qualitative or relative. The most robust parameters that can be extracted reliably from first pass techniques is rBV, which is obtained from the integral of the data time series during the first pass of the contrast agent [41]. This cannot readily be done for extra-cranial tumors because of the loss of compartmentalization of the contrast medium (see the following for further details). Instead, the time series data is fitted to a gamma-variate function from which the parameters rBV, rMTT, and rBF are derived. An additional parameter that can be derived from the T2* DCE-MRI data is the tortuosity index, which is the difference between the total time series integral and the integral of the gamma variate derived from the first pass [42]. The tortuosity index reflects the abnormal retention of contrast material due to anatomical abnormalities of the tumor vasculature described previously. The tortuosity index can only be derived for brain tumors because there is no or little loss of compartmentalization of contrast medium bolus during the first pass. Absolute quantification of T2*W DCE parameters can be obtained by measuring the changing concentration of contrast agent in feeding vessel and quantified perfusion parameters in normal brain and of low-grade gliomas [43], [44]. Absolute quantification is not currently possible for evaluation of visceral tissues and tumors owing to a number of limitations discussed later. From a practical perspective, it is not always necessary to quantify T2*-weighted DCE-MRI data to obtain insights of the spatial distribution of tissue perfusion. Simple subtraction images can demonstrate the maximal signal attenuation, which in turn has been strongly correlated with rBF and rBV in tumors [53] (Figures 2, 3, and 5). Subtraction analysis should only be done if there is no significant difference in the spatial distribution of the MTT—a feature commonly found in nonnecrotic tumors (Figures 4 and 5); this is in marked contrast to the situation in ischemia-induced cerebral stroke, where significant lengthening of

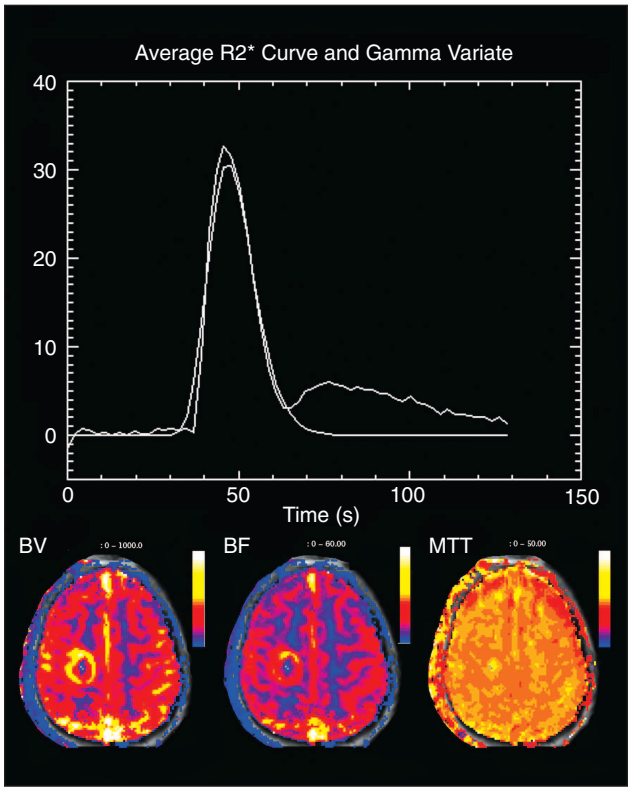

Fig. 4. Model fitting of T2*-weighted data and parametric map formation. T2* signal intensity data from Figure 2 (tumor periphery) is converted into R2* (1/T2*) and then fitted with a gamma variate function. Parametric maps representing blood flow kinetics (rBF, rBV, and MTT) are derived on a pixel-by-pixel basis. The computed values of rBV, rBF, and MTT for this region of interest are 509, 21.3 arbitrary units and 24 s.

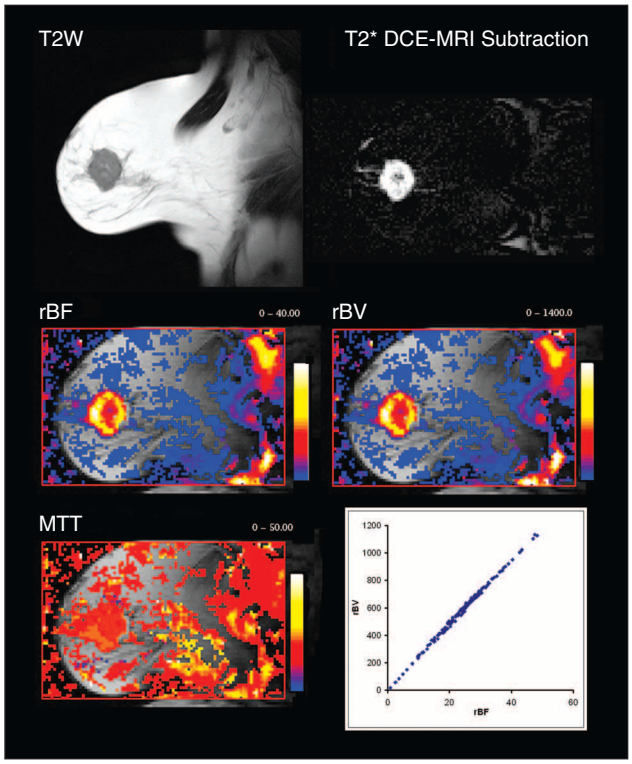

Fig. 5. Anatomic T2W and parametric DCE-MRI images of an invasive ductal cancer of the breast. This is the same tumor illustrated in Figures 3, 6, 8, and 10. T2-weighted and T2*-weighted DCE-MRI subtraction images with corresponding parametric images of rBV, rBF, and MTT. The graph shows that there is a linear correlation between blood volume and flow on a pixel level (the gradient of this line is the MTT; rBF = rBV/MTT).

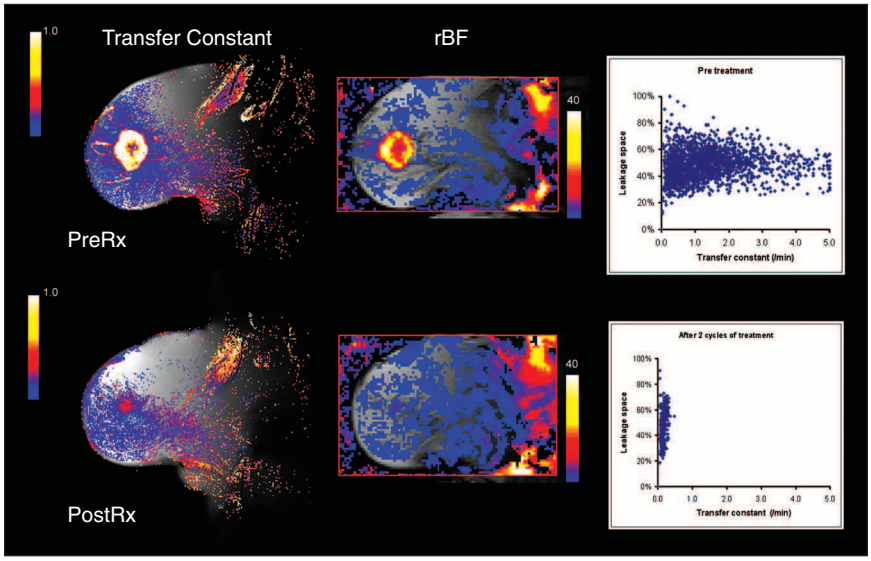

Fig. 6. Monitoring chemotherapy response of breast cancer with DCE-MRI. Fifty-two-year-old post-menopausal woman with a grade-three invasive ductal cancer of the breast. Rows depict transfer constant and rBF parametric images at identical slice positions before and after two cycles of 5-Fluorouracil, Epirubicin, Cyclophosphamide (FEC) chemotherapy. Columns depict transfer constant map (color range 0–1 min^{-1}) and relative blood flow (color range 0–40) and scatter plots of leakage space versus transfer constant. With treatment, the number of enhancing pixels is seen to decrease on the scatter plot with a reduction in relative blood flow and transfer constant. Leakage space changes are less marked. This patient had a complete clinical and radiological response to treatment after six cycles of chemotherapy.

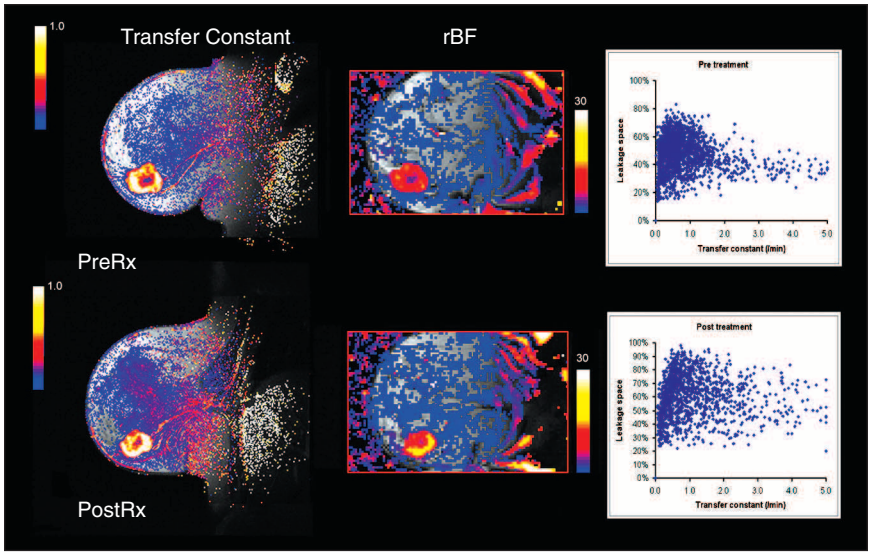

Fig. 7. Monitoring chemotherapy nonresponse of breast cancer with DCE-MRI. Thirty-nine-year-old premenopausal woman with a grade-three invasive ductal cancer of the breast. Rows depict transfer constant and rBF parametric images at identical slice positions before and after two cycles of FEC chemotherapy. Columns depict transfer constant map (color range 0–1 min^{-1}) and relative blood flow (color range 0–40) and scatter plots of leakage space versus transfer constant. With treatment, the number of enhancing pixels is unchanged on the scatter plots, and no change in transfer constant is seen on the pixel maps. There is a tendency for rBF and leakage space to increase. This patient had no clinical or radiological response to treatment after six cycles of chemotherapy and macroscopic, invasive, grade-three, ductal cancer was noted at pathological evaluation.

MTT is a characteristic feature (unchanged rBV but reduced rBF).

Limitations

Physiological effects that hinder measurements of perfusion in tumors include nonlaminar flow (which arises from the presence of irregular caliber vessels), nondichotomous branching and high vascular permeability (which leads to increased blood viscosity from hemoconcentration), and variations in the hematocrit fraction as blood passes through a vascular bed. In addition, factors such as machine stability, patient motion and intrinsic patient variables, particularly cardiac output and upstream stenoses, can affect computations. Recirculation and marked contrast leakage into the extracellular space during the first pass of contrast medium are the principle causes resulting in falsely low blood volume values. Extracranial tumors have very leaky blood vessels, and the loss of contrast medium compartmentalization is observed by the failure of the signal intensity to return to baseline. Furthermore, the T1 signal-enhancing effects of contrast medium leaking from blood vessels can counteract T2* signal-lowering effects. Quantitative imaging is thus most reliably used for normal brain and nonenhancing brain lesions because the contrast medium is completely or largely retained within the intravascular space. Solutions to overcoming these problems include the use of non-gadolinium susceptibility contrast agents based on the element dysprosium or ultrasmall superparamagnetic iron oxide particles (USPIOs), which have strong T2* effect but weak T1 effects [45], [46]. Preliminary results indicate that dysprosium-based relative cerebral blood volume (rCBV) maps are superior to those obtained with gadolinium chelates [47], [48]. USPIOs designed for bolus injection have the advantage of being retained within the vascular space during the first pass due to their larger size [49], [50]. Encouraging early clinical results using USPIOs are beginning to appear in the literature [46], [51]. Solutions for counteracting T1 enhancing effects of gadolinium chelates include idealized model fitting (gamma variate function), pre-dosing with contrast medium to saturate the leakage space, and using dual or multi-echo imaging sequences that minimize T1 sensitivity [52]. We favor

Progression to an invasive phenotype, tumor growth, and spread all depend on angiogenesis.

the latter techniques, and illustrative images of computed rBV, rBF and MTT breast and brain carcinoma is shown in Figures 4 and 5.

Clinical Experience

Quantitative imaging is currently most reliable for normal brain and nonenhancing brain lesions because the contrast medium is retained within the intravascular space. T2*-weighted perfusion mapping techniques have progressively entered neurological practice [53]–[55]. Clinical applications include characterization of tumor vascularity [56]–[59], follow-up of treatment response [44], [53], [55], [60] and the study of stroke [61]. There is a paucity of data correlating T2* kinetic parameters with MVD in human brain tumors [62], [63]. Areas of high tumor rCBV are readily visible in patients with brain gliomas (Figure 4) [58], [64] and appear to correlate with mitotic activity (information on tumor grade) and vascularity but not with cellular atypia, endothelial proliferation, necrosis, or cellularity [58]. rCBV maps appear to have a high negative predictive value in excluding the presence of a high-grade tumor in untreated patients, regardless of their enhancement characteristics on a T1-weighted MRI. In low-grade gliomas, homogeneous low rCBV is found, whereas higher-grade tumors display both low and high rCBV components [65]. rCBV can thus be used to direct a stereotactic biopsy [66], [67].

There is very little literature on the usage of T2*-weighted DCE-MRI outside the brain. Qualitative observations of signal loss observed on T2*-weighted sequences after gadolinium contrast media have been reported in preliminary clinical studies to characterize liver, breast, and brain tumors. For example, Ichikawa et al., were able to discriminate between liver metastases, haemangiomata, and hepatomas on the basis of characteristic signal intensity changes on echo-planar MRIs [68]. Both Kuhl et al. and Kvistad et al. have qualitatively evaluated the value of T2*-weighted DCE-MRI for characterizing breast lesions [69], [70]. Both studies showed strong decreases in signal intensity in malignant tissues, whereas susceptibility effects in fibroadenomas were minor. The latter studies showed that it was possible to differentiate carcinomas from fibroadenomas with high specificity using T2* characteristics, despite significant overlap in T1 enhancement patterns. The pathophysiological explanation for these observations probably relate to differences in microvessel arrangements, density, and size in malignant tumors and fibroadenomas [71]. Quantitative T2*-weighted DCE-MRIs have been used to monitor the effects of chemotherapy in breast cancer. Ah-See et al. have observed that rBV and rBF were as effective as T1-weighted kinetic parameters in predicting nonresponsiveness to treatment [72] (Figures 6 and 7).

T1-Weighted DCE-MRI

Data Acquisition

Extracellular contrast media readily diffuse from the blood into the EES of tissues at a rate determined by tissue perfusion and permeability of the capillaries and their surface area. Shortening of the T1 relaxation rate caused by contrast medi-

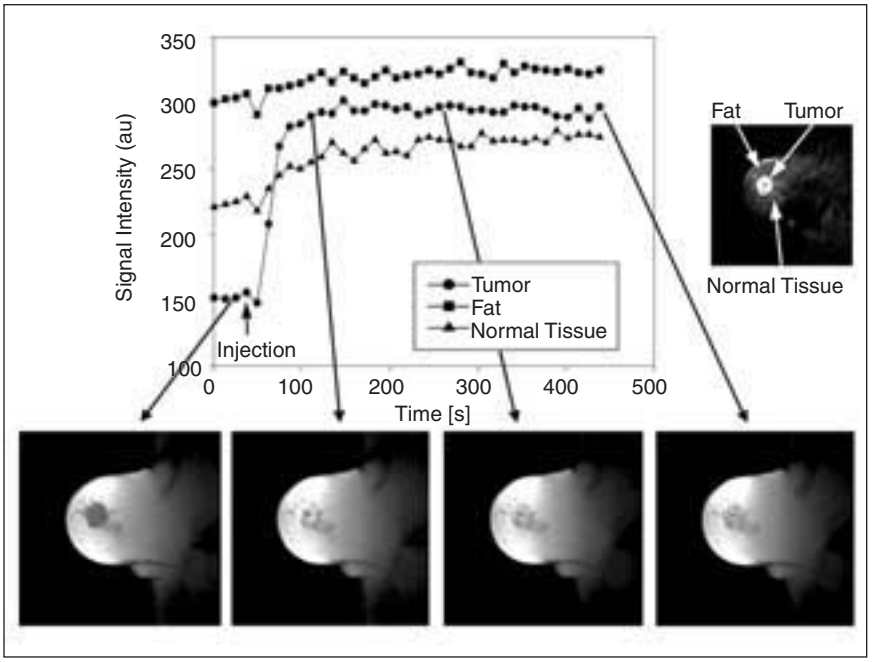

Fig. 8. Typical T1-weighted DCE-MRI study in breast tumor. Same patient as illustrated in Figures 3, 5, 6, and 10. Data from serial T1-weighted images obtained before and after the injection of 11 ml of Gd-DTPA given intravenously. Marked and sustained, early enhancement of the breast tumor is seen in the signal intensity time curves compared to the gradual enhancement of fibroglandular breast parenchyma and fat. The shape of the curve is in marked contrast to that seen on T2*-DCE-MRI in the same patient (Figure 3). Insert shows a subtraction image obtained by subtracting the 100-s image from baseline.

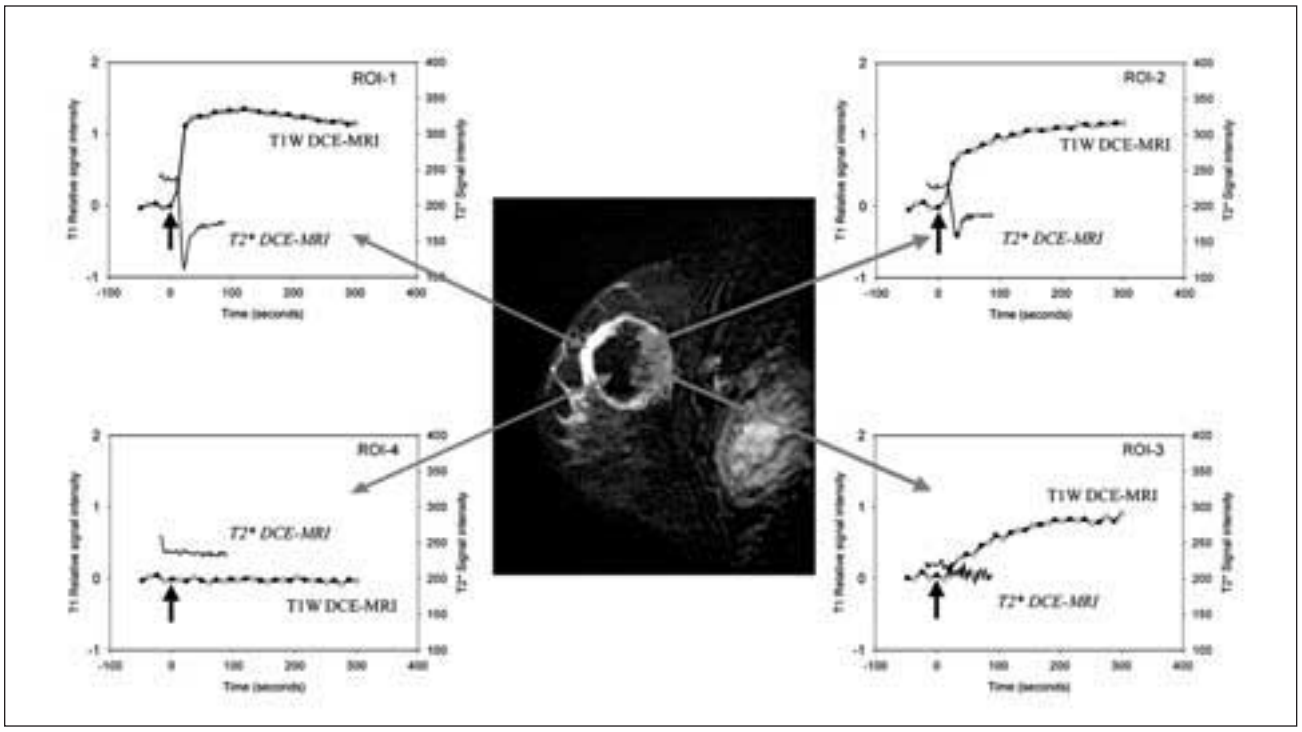

Fig. 9. Superimposing signal data from T1- and T2*-weighted DCE-MRI on the same time scale. T1-weighted subtraction (100 s post contrast medium) DCE-MRI image from a patient with a necrotic invasive ductal cancer of the breast. T1- and T2*-weighted DCE-MRI curves for the four regions of interest are superimposed on the same time scale. The zero point on the time scale represents the point of injection of contrast medium for both studies, which were performed consecutively. The onset and short duration of early T2*-weighted DCE-MRI effects corresponds precisely to the upslope on the T1-weighted enhancement curves for ROI-1 and ROI-2, confirming that the upslope has a significant vascular contribution. ROI-3 represents a small area where the flow contribution is undetectable by T2*-weighted DCE-MRI. The corresponding T1-weighted enhancement curve shape for ROI-3 is typical of one with low flow and probably reflects an area where enhancement is mostly determined by tissue permeability and microvessel surface area. ROI-4 is necrotic, and no flow is detected.

um is the mechanism of tissue enhancement. Most DCE-MRI studies employ T1-weighted gradient-echo, saturation recovery/inversion recovery snapshot sequences (e.g., turboFLASH), or echoplanar sequences (Figures 6 and 7). Each of these techniques enable tissue T1 relaxation rate to be estimated, and thus allows quantification of contrast medium concentration [73]–[75]. The choice of sequence and parameters used is dependent on intrinsic advantages and disadvantages of the sequences, taking into account T1 sensitivity, anatomical coverage, acquisition times, susceptibility to artifacts arising from magnetic field inhomogeneities, and accuracy for quantification. The amount of signal enhancement observed on T1-weighted images is dependent on a number of physiological and physical factors. Physiological factors include tissue perfusion, capillary surface area and permeability to contrast agent, and volume of the extracellular leakage space. Physical factors include native (precontrast) T1-relaxation rate of the tissue, contrast agent dose, rate of intracellular-extracellular water exchange, imaging sequence parameters used, and measurement gain and scaling factors.

T1-weighted kinetic enhancement curves have three distinct phases; the upslope, maximum enhancement, and washout (Figures 8 and 9). It is generally recognized that the upslope is highly dependent on tissue perfusion and permeability with perfusion predominating. Maximum enhancement is related to the total uptake concentration of the contrast medium in the interstitial space, and washout rate is associated with tissue contrast agent concentration decrease and is strongly related to vascular permeability. If it is assumed that tissue enhancement has contributions from vascular and extravascular compartments (see compartmental modeling under the section "Quantification," below), then it is possible to separate these inputs mathematically using deconvolution techniques [76], which is helpful for understanding the shape of kinetic curves [77]. The dominant contribution of perfusion to the upslope of T1-weighted DCE-MRI enhancement curves can be verified empirically by correlating T1- and T2*-weighted DCE-MRI enhancement curves and corresponding kinetic pixel maps [52]. Figure 9 displays kinetic enhancement from several regions of interest (ROIs) shown on the same time scale, although the image datasets were acquired sequentially (T1- followed by T2*-weighted DCE-MRI). It can be seen that the steep initial upslopes on T1-weighted enhancement curves with the greatest signal intensity decreases on T2*-weighted DCE-MRI. The onset and short duration of these early T2*-weighted DCE-MRI effects corresponds precisely to the upslope on the T1-weighted enhancement curves, confirming that the upslope has a significant vascular contribution.

Quantification

Signal enhancement seen on T1-weighted DCE-MRI can be assessed in two ways: by the analysis of signal intensity changes (semiquantitative) and/or by quantifying tissue T1 relativity (R1) or contrast agent concentration change using phar-

macokinetic modeling techniques. Semiquantitative parameters describe signal intensity changes using a number of descriptors. These parameters include curve shape [78], [79], onset time (time from injection or appearance in an artery to the arrival of contrast medium in the tissue of interest), gradient of the upslope of enhancement curves, maximum signal intensity, and washout gradient. As the rate of enhancement has been shown to be important for improving the specificity of clinical diagnoses, parameters that include a timing element are often used (e.g., maximum intensity time ratio (MITR) [80] and maximum focal enhancement at one minute [81], [82]. The uptake integral or initial area under the signal intensity curve (IAUC) or gadolinium contrast medium concentration (IAUGC) curve also has been studied [83]. IAUGC is a relatively robust and simple technique, which characterizes all enhancing regions without the problems associated with model fitting failures in pharmacokinetic model derived parametric images (see the following). However, IAUGC does not have a simple relationship to the physiology parameters of interest (perfusion, permeability, and leakage space). Experimental data indicates that, in practice, IAUGC at 30 s correlates with K^{trans}, whereas IAUGC at 90 s correlates with lesion leakage space (v_e) in brain tumors [84]. Thus, semiquantitative parameters have a close but complex and not totally defined link to underlying tissue physiology. Semiquantitative parameters have the advantage of being relatively straightforward to calculate, but they have limitations. These limitations include the fact that they do not accurately reflect contrast medium concentration in tissues and can be influenced by scanner settings (including gain and scaling factors). These factors limit the usefulness of semiquantitative parameters and make between-patient and between-system comparisons difficult.

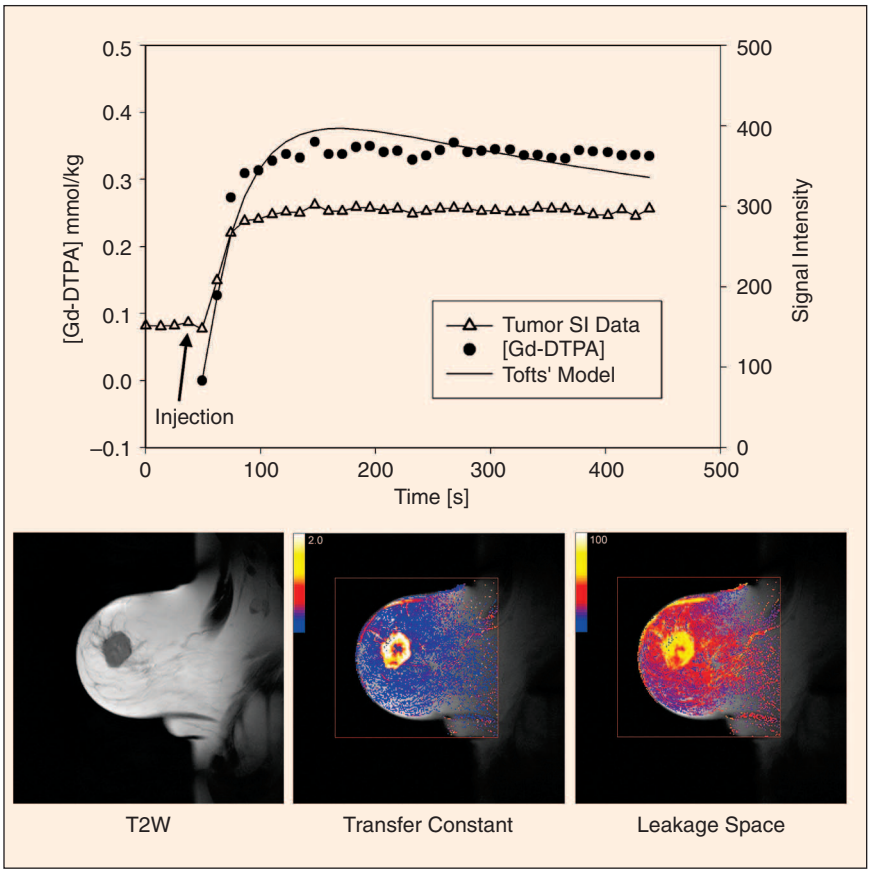

Fig. 10. Converting signal intensity into contrast concentration and model fitting. Data obtained from the patient as illustrated in Figures 3, 5, 6, and 8. Contrast medium injection (11 ml of Gd-DTPA) took place after the third data point. Quantification of time signal intensity data (Δ) into contrast agent concentration (•) is performed first according to the method described by Parker et al. (75). The model-fitting procedure (continuous line) is done using with the Tofts' model (86). Note that model fitting to contrast agent concentration data is not perfect. Calculated quantified parameters are transfer constant = 0.82 min^{-1}, leakage space 47%, rate constant = 1.74 min^{-1}). Anatomic T2W images and parametric transfer constant (color scale 0–2 min^{-1}) and leakage space (color scale 0-100%) are also shown.

Quantitative techniques use pharmacokinetic modeling applied to changes in tissue contrast agent concentration or R1. In general, it is not recommended that pharmacokinetic modeling be done on signal intensity data unless it is has been shown that there is a direct relationship between signal intensity and contrast agent concentration over the entire range expected in tissues. Signal intensity changes observed during dynamic acquisition are used to estimate contrast agent concentration in vivo, following measurements that enable the precontrast native T1 of the tissues to be obtained [75], [85]. Concentration-time curves are then mathematically fitted using one of a number of recognized pharmacokinetic models, principally those of Larsson, Tofts, and Kermode [86], [87] (Figure 9). Quantitative pharmacokinetic parameters are derived from the following expression: $c(t) = K_{trans} \cdot C_a(t) \oplus e^{-K_{ep} \cdot t}$; where C(t) is the tissue concentration of contrast media, $C_a(t)$ is the arterial concentration, and K_{trans} and K_{ep} are rate constants. This is a generalized kinetic model derived from the Kety model by Larsson et al. In the Tofts model, a standardized vascular input function [88] is used resulting in the following expression:

$$C(t) = D \cdot K_{trans} \cdot \sum_{i=1}^{2} a_i \cdot \frac{\left[e^{-\left(\frac{K_{trans}}{Ve}\right) \cdot (t - t_o)} - e^{-m_i \cdot (t - t_o)} \right]}{m_i - \left(\frac{K_{trans}}{Ve}\right)}$$

where D = dose of contrast media, m_i is a rate constant for vascular elimination, and a_i is a physiologically derived constant. The response of a step change in arterial plasma concentration, 0 to C_{p0} at time $t = 0$, is $C(t) = Ve \cdot C_{p0} \cdot (1 - e^{-K_{ep} \cdot t})$, where C_{p0} is the plasma concentration. This expression is

convenient to use for modeling the shape of the concentration time curve following a short bolus of contrast media and reliable estimates of K_{ep} being obtained. For a detailed discussion on pharmacokinetic modeling techniques, readers are directed to the review by Tofts [89] and a detailed analysis of the data acquisition methodology, which has been reviewed by Dale et al [90]. Figure 11 shows examples of parametric images derived from both Larsson's and Tofts' model approaches in rectal cancer. Examples of modeling parameters include the volume transfer constant of the contrast agent (K^{trans}—formally called permeability-surface area product per unit volume of tissue—unit minute^{-1}), leakage space as a percentage of unit volume of tissue (v_e—unit %), and the rate constant (k_{ep} also called K_{21}—unit minutes^{-1}) (Figure 1). These standard parameters are related mathematically ($k_{ep} = K^{trans}/v_e$) [30].

It is important to note that the physiological meaning of K^{trans} is dependent on the underlying behavior of the tissue microvessels. Where the PS is high compared with flow (F), these tissues are described as being "flow limited." In these areas, K^{trans} estimates are dominated by plasma flow [($K^{trans} = Fp(1\text{-}Hct)$, where p is the tissue density and 1-Hct (hematocrit) is the plasma fraction]. When permeability is low compared to flow, these tissues are described as being "permeability limited," and $K^{trans} = PS$. The mixed situation occurs most commonly in tumors, so neither flow nor permeability predominates; for extracellular gadolinium containing chelates, such as Gd-DTPA, there is a tendency for the influence F to outweigh PS. Evidence that K^{trans} is dominated by flow in extracranial tumors is now emerging (see also limitations following). Recently, Kiessling at al. reported a strong positive correlation between microbubble enhanced Doppler ultrasound and dynamic T1-weighted DCE-MRI kinetic parameters [91]. Previously, it has been shown that there is a near linear correlation between microbubble velocity measured on Doppler ultrasound and red blood cell velocity [92]. Both Lancester et al. and Ah-See et al. have shown strong positive correlations between K^{trans} and rBF derived from T1- and T2*-weighted DCE-MRI in pelvic and breast cancer, respectively [93] (Lancester K, personnel communication). Further corroboration comes from the work of Maxwell et al., who compared T1-weighted DCE-MRI kinetic parameters with tumor blood flow measured by the uptake of radiolabeled iodoantipyrine (IAP) in rat carcinosarcomas [94]. They showed that the time-course of changes in K^{trans} and the area under curve (AUC) as measured by DCE-MRI, and tumor blood flow rate measured by IAP uptake after treatment with a vascular targeting compound (Combretastatin—CA4P) were highly correlated, although the changes in K^{trans} and AUC were smaller than those in blood flow by IAP. Maxwell et al. concluded that DCE-MRI relatively underestimated the magnitude of the effect on blood flow, probably due to leakage of contrast media.

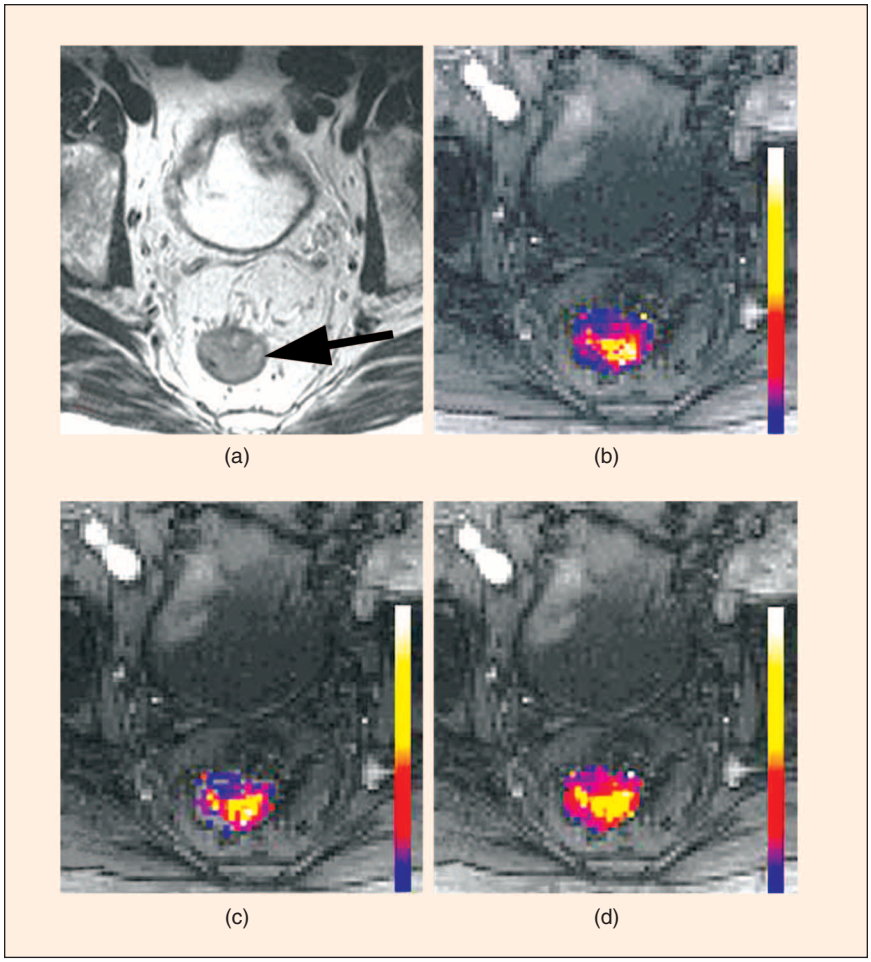

Fig. 11. Rectal cancer: modeling approaches compared. (a) Anatomical T2-weighted image of a rectal cancer (arrow). Parametric images of the rate constant (k_{ep}) derived from the same data using three different model approaches. (b) General response. (c) Tofts' model using standard vascular input function. (D) Tofts' model using the Larsson model with an input function obtained from the external iliac artery. A high degree of concordance between the images is seen.

Limitations

Quantitative parameters are more complicated to derive compared with those derived semiquantitatively, which deters their use at the workbench. Difficulties arise from more complex data acquisition requirements and by the lack of available software to analyze acquired data. The model chosen may not exactly fit the data obtained (Figure 10), and each model makes a number of assumptions that may not be valid for every tissue or tumor type [30], [89]. From the previous discussions, it is clear that there are uncertainties with regard to the reliability of kinetic parameter estimates derived from the application of tracer kinetic models to T1-weighted DCE-MRI data [95]–[97]. These derive from assumptions implicit in kinetic models and the measurement of tissue contrast agent concentration [90]. For example, the Tofts model uses a standard description of the time varying blood concentration of contrast agent [88] and assumes that the supply of contrast medium is not

flow limited and that tissue blood volume contributes negligibly to signal intensity changes compared to that arising from contrast medium in the interstitial space. As already noted previously, this is not universally true in extracranial tumors; Figure 9 is a good example where the vascular contribution to the T1 tissue enhancement curve is obviously sizeable. Buckley has suggested that the application of commonly accepted models and their respective model-based assumptions to DCE-MRI data leads to systematic overestimation of K^{trans} in tumors [98]. Thus, it is difficult to be certain about how accurately model-based kinetic parameter estimates compare with the physiological parameter that they purport to measure, particularly as there is no reliable clinical gold standard.

Despite these complexities, it is important to remember that quantitative kinetic parameters can provide insights into underlying tissue pathophysiological processes that semiquantitative descriptors cannot. If the time varying contrast agent concentration can be measured accurately, and the type, volume, and method of administration of contrast agent are consistent, then it is be possible to directly compare pharmacokinetic parameters acquired serially in a given patient and in different patients imaged at the same or different scanning sites. Furthermore, it is possible to use quantitative DCE-MRI as a tool for decision making, as attested to by extensive clinical experience (see the following).

Validation

Many studies have attempted to correlate tissue MR enhancement with immuno-histochemical MVD measurements in a variety of tumors. Some MRI studies have shown broad correlations between T1 kinetic parameters estimates and MVD [91], [99]–[104], whereas others have found no correlation [77], [105], [106]. Recently, VEGF a potent vascular permeability and angiogenic factor, has been implicated as an additional explanatory factor that determines MR signal enhancement. Knopp et al. reported that MRI vascular permeability to contrast media closely correlated with tissue VEGF expression in breast tumors [107], whereas Su et al did not [77]. The importance of the role of VEGF in determining MR enhancement is supported by the spatial association of hyperpermeable capillaries detected by macromolecular contrast enhanced MRI and VEGF expression on histological specimens [108]. Furthermore, the observation that T1-weighted DCE-MRI measurements can detect

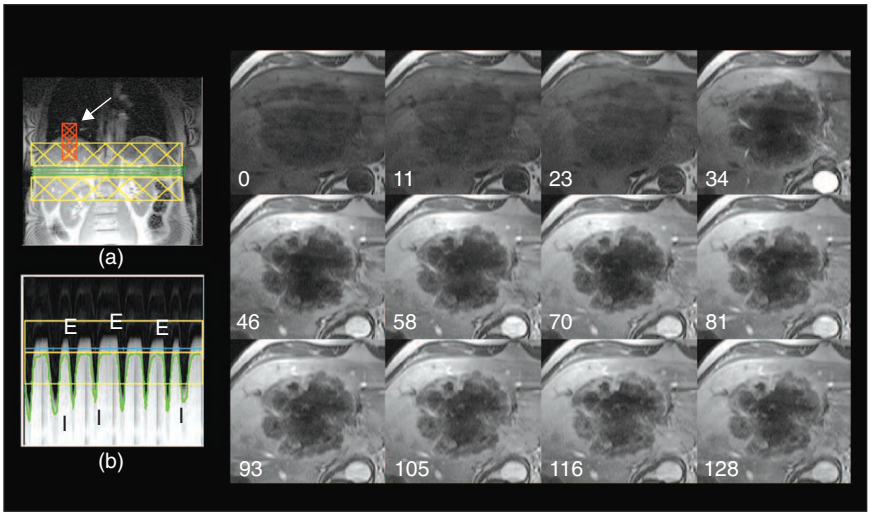

Fig. 12. Navigator-guided T1-weighted DCE-MRI of liver metastases. A navigator gradient-recalled echo (GRE) sequence was used for DCE-MRI of liver metastases. a) Scout view showing slice positions, saturation bands, and navigator band (arrowed) at the interface between lung and liver. b) Corresponding navigator trace over a period of 90s. Some inhales (I) and exhales (E) are marked. The collage shows magnified images of one of three image slices from the injection through to +128 s. There was very little motion artefact from chest wall motion. Some motion blurring of the left hepatic lobe was seen due to transmitted cardiac pulsations.

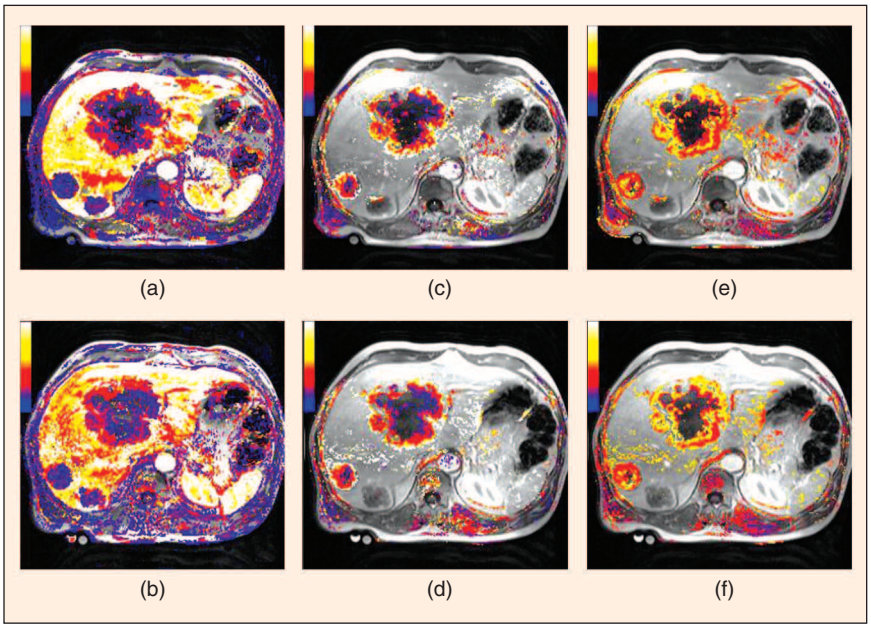

Fig. 13. Quantitative and semiquantitative images showing reproducibility of liver DCE-MRI. Semiquantitative mean gradient ((a), (b)) and quantitative ((c), (d): K^{trans} maps, scale 0–1 min^{-1} and (e), (f): v_e maps, scale 1–100%) calculated images for the same patient as in Figure 12 on two consecutive days. The mean gradient image shows that liver enhancement is greater than the tumors in this patient. No color is seen in normal liver on the K^{trans} map because of modeling failures related to hypervascularity/dual blood supply. Modeling failures due to high vascular volume also account for lack of color in the kidney. The follow-up images on subsequent days showed excellent slice reproducibility.

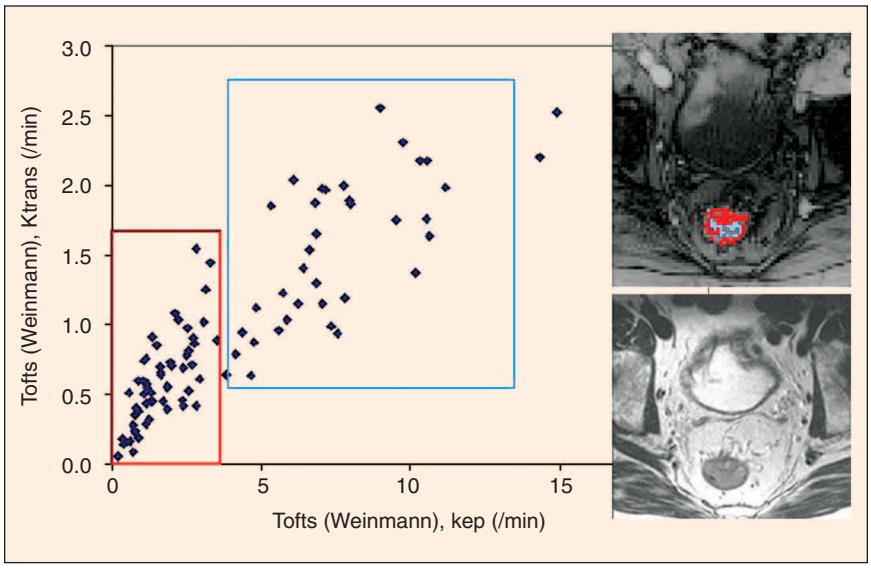

Fig. 14. Mapping tumor kinetics to anatomical features. Scatter plot of transfer constant (K^{trans}) and rate constant (k_{ep}) in a patient with rectal cancer using the Tofts' model with a Weinmann input function. Two distinct clusters highlighted in red and blue are identified and indicated in red and blue on the graph. The voxels in each cluster are mapped back onto the anatomic images using the same colors.

changes in flow and permeability after anti-VEGF antibody, after the administration of inhibitors of VEGF signaling, in xenografts [109]–[112], and in humans [113]–[115] lends weight to the important role played by VEGF in determining MR enhancement. Other tissue characteristics that have been correlated with T1-weighted enhancement patterns include the degree of stromal cellularity and fibrosis [116], [117] tissue oxygenation [106], [118] and tumor proliferation [101], [119].

Clinical Experience

Analysis of enhancement seen on T1-weighted DCE-MRI is a valuable diagnostic tool in a number of clinical situations. The most established role is in lesion characterization, where it has found a role in distinguishing benign from malignant breast and musculoskeletal lesions [78]–[82], [120]. In the brain, T1 DCE-MRI can be used to noninvasively grade brain tumors [121]–[123]. Dynamic T1-weighted MRI studies have also been found to be of value in staging gynecological malignancies and bladder and prostate cancers [124]–[127]. Recently, enhancement parameters have been shown to predict prognosis in patients with cervix cancers [128]. DCE-MRI studies have also been found to be of value in detecting tumor relapse in the presence of fibrosis within treated tissues of the breast and pelvis [129]–[136]. DCE-MRI is also able to predict response to or monitor the effects of a variety of treatments. These include neoadjuvant chemotherapy in bladder and breast cancers and bone sarcomas [137]–[140]. Other treatments that can be monitored include radiotherapy in rectal and cervix cancers [141]–[144], androgen deprivation in prostate cancer [145], and vascular embolization of uterine fibroids [146]–[148]. Recently, DCE-MRI has been used to monitor the effects of antivascular anticancer drugs [113]–[115], [149]–[151]. It is noteworthy that enhancement on DCE-MRI can be affected by most types of successful treatments. This reflects on the fact that tumor cells kill; no matter how achieved, they ultimately result in vascular shutdown, probably because of the loss of proangiogenic cytokine support, which results in apoptosis of proliferating endothelial cells.

Challenges for Perfusion DCE-MRI

For DCE-MRI, it is recognized that high-resolution and short imaging-time are competing examination strategies on current equipment and software. Higher temporal resolution imaging necessitates reduced spatial resolution, decreased anatomic coverage, or a combination of them. Accuracy in the parameters derived from DCE-MRI are dependent on the image acquisition rate, as can be seen from the following expression

$$E = \sqrt{\sum_{i=1}^{N} \frac{\left(C_i^2 - c_i^2\right)^2}{N - P}}$$

where E is the error, N the number of sample data points, P the number of free parameters in the model, C_i is the contrast media concentration, and c_i is the model estimate of the contrast media concentration [152]. From this expression, we can immediately see that a small number of sample points, N, leads to large error estimates. High spatial resolution will, by necessity, reduce the number of data samples, leading to increased error estimates. Additionally, the finer the spatial resolution, the greater the need for accurate image registration, as misregistration will result in increased motion induced noise in data. Conversely, a large number of data samples acquired at a high sampling rate reduces the error and enables more complex models with a greater number of free variables to be used in the model fitting process. Thus, compromises have to be made trading temporal resolution against coverage and spatial resolution. Higher temporal resolution techniques are essential for T2*-weighted DCE-MRI and appear to improve specificity of T1-weighted examinations because of better characterization of tissue enhancement [153]. Even though data collection procedures for quantitative examinations differ to those used in routine clinical practice, there is debate as to which technique(s) is/are best [154]–[156]. The MRI community needs to agree on a limited number of examination and analysis protocols in order to enable DCE-MRI to be more completely validated and used in clinical trials. Both generic and organ specific consensus methods for quantified T1-weighted DCE-MRI data collection have been published [23], [157], [158].

A major source of variability in the DCE-MRI literature relates to the method of contrast administration. The dose and method of administration of contrast agent affects modeling procedures and clinical results. Typically, contrast agents are given either as a bolus [86] or infusion [159]. When a powered injector is used, reproducible injections are ensured. Short injection times are optimal for fast DCE-MRI imaging techniques, especially when evaluating lesions with high microvessel permeability for ECF contrast agents [160], [161] but conversely, slower infusion methods may be better when

the temporal resolution of the study is longer and volume coverage is being undertaken [154]. The method of ECF contrast medium administration also needs to be tailored to the sequence used and sequence sensitivity to T2* and T1 effects [162]–[164]. Using injection rates of 5 ml/s can reduce the T1 and T2 relaxation times in blood to the order of 10 ms during the first pass of the contrast media [165]. Gradient echo sequences using echo times of the order of 10 ms will be subject to significant T2 related attenuation that will require correction in quantitative analysis methods. The current trend in DCE-MRI is to acquire data in three-dimensional (3D) volumes; this requires the use of both short repetition times (TR) and short echo times (TE). The short TR requires that DCE-MRI data are acquired with a small nutation angles for excitation. There are two reasons for this; to reduce the specific absorption rate of electromagnetic energy in the body (a safety reason) and to ensure that the signal obtained is related to the actual concentration of contrast media. A consequence of this is that a number of precontrast measurements with differing nutation angles are required to obtain sufficient data for the calculation of the initial tissue relaxation rate (R1). However, small nutation angles also reduce the SNR of the measurement, which can be compensated for in part by the SNR advantage of obtaining 3D volumes.

Another issue that needs to be addressed is that of data collection in body parts where there is a large degree of physiological movement, such as the lungs and liver. The presence of motion can invalidate functional vascular parameter estimates, particularly for pixel-by-pixel analyses. Methods for overcoming/minimizing these effects include the application of navigator techniques [166] (Figure 12) or imaging in the nonaxial plane using sequential breath holds during data acquisition and subsequently registering the data prior to analysis [167]. The latter method has the advantage that a fixed time interval between measurements is maintained. Sophisticated image registration methods have also been used to eliminate misregistration and motion induced noise in DCE-MRI studies in breast [168].

A practical question often asked is whether it is necessary to quantify imaging data to answer important clinical questions. Simple morphologic and semiquantitative analyses seem to work well in the clinic. However, it is important to realize that semiquantitative diagnostic criteria cannot be simply applied from one center to another, particularly when different equipment and sequences are used. Quantification techniques aim to minimize errors that can result from the use of different equipment and imaging protocols. Quantification techniques also enable the derivation of kinetic parameters that are based on some understanding of physiological processes, and so can provide insights into tumor biology (see previous). Quantification techniques are therefore preferred when evaluating antivascular anticancer [169]. Quantification techniques rely on the fitting of the data acquired to a mathematical model. Experience shows that the model chosen may not fit the data acquired (Figure 13) (modeling failures) and that apparently sensible kinetic values can be obtained even from noisy data. The causes of modeling failures are complex and often not well understood. Reasons include high vascular permeability (i.e. when the intravascular

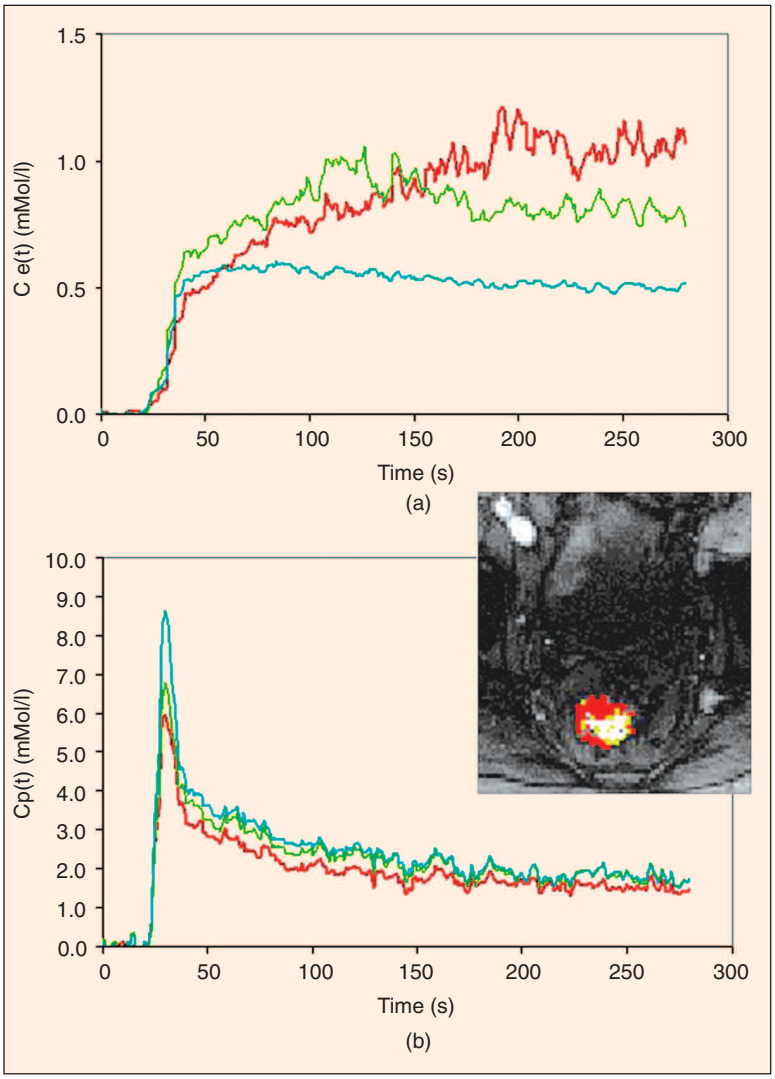

Fig. 15. Separating tumor perfusion from permeability using combined T1- and T2*-weighted DCE-MRI. Gd-DTPA concentration times curves obtained from patient with rectal cancer (same patient shown in Figures 11 and 14), calculated by the use of T1- and T2*-weighted methods derived from a single dual-gradient echo sequence (52). Gd-DTPA concentration changes from T1-weighted DCE-MRI imaging is shown on the top panel and that obtained from T2*-weighted imaging DCE-MRI on the bottom panel. The curves in both panels show the average curves for the corresponding color coded regions within the tumor (anatomical image inset). The tumor was segmented by cluster analysis using estimates of rate constant (k_{ep}) derived from two model fitting methods, one including an input function and one not. The most striking aspect of the segmentation is the selection of three completely different time series in the data derived from the T1 DCE-MRI data, with only minor variations in the concentrations calculated with R2 (i.e., equivalent input functions). This suggests that permeability of Gd-DTPA within each of these tumor regions is widely different.

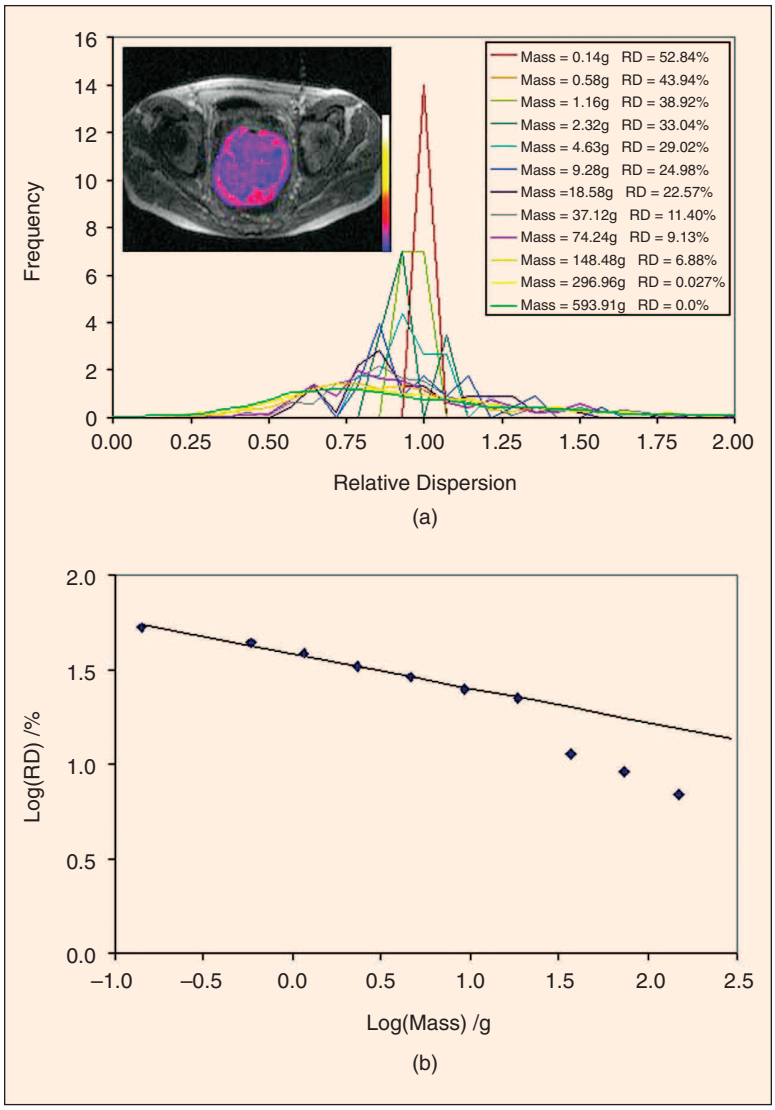

Fig. 16. Fractal analysis of tumor heterogeneity. Bottom panel depicts a log relative dispersion (standard deviation/mean) plots of the AUC T2* (rBV) on the Y axis and the log of the mass element sampled on the X axis of a patient with rectal cancer. The mass element is obtained from the pixel dimensions and multiplied by the tissue density, which is assumed to be 1.06 g per cm^3. The relative dispersion histogram is shown in the top panel. The relative dispersion ranges from 0% with the whole of the region of interest included to 52.84% for the smallest mass sample—an individual pixel. Relative dispersion is an ideal method to characterize heterogeneity in parametric images.

contrast medium concentration cannot be maintained due to markedly leaky vessels in the setting of limited blood flow), high tissue blood volumes, multiple tissue compartments, and an incorrect or assumed arterial input function. Modeling failures would be reduced if the arterial input function (AIF) is measured and used to estimate kinetic parameters. Fitting data with the Tofts model can be improved if patient derived vascular input functions are used as inputs in the pharmacokinetic model in place of the standard Weinmann coefficients [88]. Reliable methods for measuring AIF for routine DCE-MRI studies are now emerging, but are still not widely available [170]. The use of AUC for both T1 and T2* data overcomes the issue of characterizing pixels that fail to fit a model, a major problem found in pharmacokinetic model based approaches.

Inevitably, the future will yield kinetic models of increasing sophistication—for example, the effects of variable proton exchange rates are yet to be incorporated into a model of contrast agent uptake. We do not have models that fit all data types, and more sophisticated models that provide insights into tissue compartment behavior are needed [30], [162]. It is probably true that modeling approaches currently are not always applied to suitable data in ways that are robust to over-fitting, systematic errors, and noise. The application of more sophisticated models available in the literature requires superior scanning methods to achieve their full potential. The combination of three Tesla scanning and parallel imaging techniques will allow very rapid data acquisition of suitable SNR to allow increased accuracy and precision in quantitative DCE-MRI.

Variation between measurements of the same quantity on the same individual can be caused either by random measurement error or by physiological changes between measurements. While it is possible (in theory) to reduce measurement error, physiological variation is inherent and can cause difficulty in attempts to characterize disease or to monitor the effects of therapy. An estimate of measurement error enables us to decide whether a change in observation represents a real change. Data addressing the precision and measurement variability of DCE-MRI techniques is urgently needed and should be an integral part of any prospective study that evaluates functional response to therapy [42], [171]–[173]**.** Where possible, and in the absence of existing reproducibility of data specific to the method, two baseline studies should be incorporated into the trial design to allow assessment for individual patient (Figure 13) and group reproducibility. A standardized statistical approach should also be used to be able to compare the precision and measurement variability between and within centers [169]. Such assessments should ideally be made for each study involving new (or modified) acquisition procedures, new patient groups, or analysis methods. Factors that determine measurement error for a given technique also need to be defined. These include imaging instrumentation and set-up procedures, imaging technique used, contrast injection protocol, modeling techniques (including assumptions), and AIF and cardiac output [170].

Analysis and presentation of imaging data needs to take into account the heterogeneity of tumor vascular characteristics. User-defined whole tumor ROIs yield graphical outputs with good SNR, but they lack spatial resolution and are prone to partial volume averaging errors and thus are unable to evaluate tumor heterogeneity. As a result, whole tumor ROIs may not reflect small areas of rapid change and so may be insensitive to drug action. Many authors have commented that whole tumor ROI assessment may be inappropriate, par-

ticularly for the evaluation of malignant lesions, where heterogeneous areas of enhancement are diagnostically important [58], [75], [82].

Pixel mapping has a number of advantages, including the appreciation of heterogeneity of enhancement and removal for the need to selective place user-defined ROIs. The risk of missing important diagnostic information and of creating ROIs that contain more than one tissue type is reduced. An important advantage of pixel mapping is being able to spatially match tumor vascular characteristics, such as blood volume, blood flow, permeability, and leakage space (Figures 14 and 15)**.** Such displays provide unique insights into tumor structure, function, and response (Figures 6 and 7). Pixel mapping techniques have the disadvantages of having poor SNRs and require specialist software for their generation. While visual appreciation of heterogeneity is improved by pixel mapping displays, quantification of the same can be more difficult. Recently, histogram and principal components analysis has been used to quantify the heterogeneity of tumors for comparative and longitudinal studies, for monitoring the effects of treatment, and to show the regression or development of angiogenic hot spots [143], [174]. Other approaches to characterize tumor heterogeneity in parametric maps include the application of fractal statistics. Relative dispersion provides a powerful method of reducing the complex data to a simple scaling relationship [175]. Relative dispersion (RD) is defined as the standard deviation divided by the mean value. The relative dispersion histogram is formed by calculating relative dispersion over a range of pixel sizes (often converted to mass by appropriate scaling). The scaling relationship is found from the slope of the log(RD) versus the log(mass). This method demonstrates that the parametric data from tumors exhbit fractal properties [176] (Figure 16).

Conclusions

There are definite clinical requirements to develop noninvasive imaging assays of tumor angiogenesis. DCE-MRI is the favored technique for evaluating tumors with respect to their state of the functional microcirculation. Depending on the technique used, data reflecting tissue perfusion (blood flow, blood volume, MTT), microvessel permeability surface area product, and extracellular leakage space can be obtained. Insights into these physiological processes can be obtained from inspection of kinetic enhancement curves or by the application of complex compartmental modeling techniques. The accuracy of clinical diagnoses can be increased by combining both morphological and kinetic features. Angiogenesis imaging techniques potentially have widespread clinical applications, and their recent development has been spurred on by the development of antivascular anticancer approaches. A realistic appraisal of the strengths and limitations of DCE-MRI techniques is required, and a number of challenges must be met if DCE-MRI is to enter into widespread clinical practice. These include the need for commercial equipment manufacturers to provide robust methods for rapidly measuring time varying change in T1 relaxation rates, incorporation of AIF into kinetic modeling processes, robust analysis software that allows input from a variety of MRI devices and validated statistical tools for the evaluation of heterogeneity. Such developments will be essential for multicenter trials, where it will be necessary to establish effective cross-site standardization of measurements and evaluation. Imaging scientists, radiologists, and clinicians will need to become enthusiastic key players if there is to be successful clinical implementation of DCE-MRI.

Acknowledgments

We are grateful to Dr. Jane Taylor and Simon Walker for their assistance in the preparation of the illustrative material for this review. Parametric calculations and images were produced by MRI software (MRIW) developed at the Institute of Cancer Research, Royal Marsden Hospital, London. The support of Cancer Research UK and the Childwick Trust, who support the work of the Clinical Magnetic Resonance Research Group at the Royal Marsden Hospital and at the Paul Strickland Scanner Center, Mount Vernon Hospital, respectively, is gratefully acknowledged.

David J. Collins is Principal Clinical Scientist at the Cancer Research United Kingdom (CRUK) Clinical Magnetic Resonance Research Group, Royal Marsden Hospital, Sutton U.K. Having originally trained in electrical engineering and physics, he moved on to medical physics research in 1986 at the Royal Marsden Hospital. He is currently responsible for developing, multifunctional magnetic resonance and functional computer tomography imaging studies in cancer patients. Additional research interests are localized magnetic resonance correlation spectroscopy studies in cancer patients. He is a member of several institutions, the International Society of Magnetic Resonance in Medicine, Institute of Physics, and the British Institute of Radiology.

Anwar R. Padhani is a clinical radiologist at Mount Vernon Cancer Treatment Centre and an honorary senior lecturer at University College, London. His clinical interests include the use of MRI, CT, functional, and 3D imaging in cancer. He is an expert in a number of emerging MRI applications, including dynamic and breast MRI and MR lymphography. His research focus is on translational work aimed at obtaining functional information on the microenvironment of human tumors (blood flow, permeability, and oxygenation). This work, which involves CT scanning, MRI, and PET, is of international renown. He is a member of the Study Advisory Group steering the U.K. Multi-Centre Study of MRI Screening in women at High Genetic Risk of breast cancer (MARIBS). He has helped establish that dynamic MRI perfusion can act as a surrogate marker of tumor response to antivascular/antiangiogenic therapies. He is a member of a working panel that advises CRUK on the imaging requirements for future antiangiogenesis clinical trials. He has given numerous lectures at national and international meetings,, including the International Society of Magnetic Resonance in Medicine, Radiological Society of North America, and European Congress of Radiology. He is deputy editor (medical) of the British Journal of Radiology.

Address for Correspondence: David J. Collins, Cancer Research UK Clinical Magnetic Resonance Research Group, Institute of Cancer Research and The Royal Marsden NHS Trust, Sutton, Surrey, United Kingdom. Phone: ++44-(0)20-8661-3701. Fax: ++44-(0) 20-8661-0846. E-mail: David.Collins@icr.ac.uk.

References

[1] E.M. Conway, D. Collen, and P. Carmeliet, "Molecular mechanisms of blood vessel growth," *Cardiovasc. Res.*, vol. 49, no. 3, pp. 507–521, 2001.

[2] J. Folkman, "Angiogenesis in cancer, vascular, rheumatoid and other disease," *Nat. Med.*, vol. 1, no. 1, pp. 27–31, 1995.

[3] M. Neeman, J.M. Provenzale, and M.W. Dewhirst, "Magnetic resonance imaging applications in the evaluation of tumor angiogenesis," *Semin. Radiat. Oncol.*, vol. 11, no. 1, pp. 70–82, 2001.

[4] H.F. Dvorak, J.A. Nagy, D. Feng, L.F. Brown, and A.M. Dvorak, "Vascular permeability factor/vascular endothelial growth factor and the significance of microvascular hyperpermeability in angiogenesis," *Curr. Top. Microbiol. Immunol.*, vol. 237, pp. 97–132, 1999.

[5] L.E. Benjamin, D. Golijanin, A. Itin, D. Pode, and E. Keshet, "Selective ablation of immature blood vessels in established human tumors follows vascular endothelial growth factor withdrawal," *J. Clin. Invest.*, vol. 103, no. 2, pp. 159–165,1999.

[6] M.W. Dewhirst, "Angiogenesis and blood flow in solid tumors," in *Drug Resistance in Oncology*, B. Teicher, Ed. New York: Marcel Dekker, 1993, pp. 3–24.

[7] R.D. Braun, J.L. Lanzen, and M.W. Dewhirst, "Fourier analysis of fluctuations of oxygen tension and blood flow in R3230Ac tumors and muscle in rats," *Amer. J. Physiol.*, vol. 277, no. 2, pt. 2, pp. H551–H568, 1999.

[8] J. Folkman, "New perspectives in clinical oncology from angiogenesis research," *Eur. J. Cancer*, vol. 32A, no. 14, pp. 2534–2539, 1996.

[9] J.W. Rak, B.D. St. Croix, and R.S. Kerbel, "Consequences of angiogenesis for tumor progression, metastasis and cancer therapy," *Anticancer Drugs*, vol. 6, no. 1, pp. 3–18, 1995.

[10] R. Gilles, B. Zafrani, J.M. Guinebretiere, M. Meunier, O. Lucidarme, A.A. Tardivon, F. Rochard, D. Vanel, S. Neuenschwander, and R. Arriagada, "Ductal carcinoma in situ: MR imaging-histopathologic correlation," *Radiology*, vol. 196, no. 2, pp. 415–419, 1995.

[11] Y.N. Park, Y.B. Kim, K.M. Yang, and C. Park, "Increased expression of vascular endothelial growth factor and angiogenesis in the early stage of multistep hepatocarcinogenesis," *Arch. Pathol. Lab. Med.*, vol. 124, no. 7, pp. 1061–1065, 2000.

[12] G. Gasparini, M. Toi, R. Miceli, P.B. Vermeulen, R. Dittadi, E. Biganzoli, A. Morabito, M. Fanelli, C. Gatti, H. Suzuki, T. Tominaga, L.Y. Dirix, and M. Gion, "Clinical relevance of vascular endothelial growth factor and thymidine phosphorylase in patients with node-positive breast cancer treated with either adjuvant chemotherapy or hormone therapy," *Cancer J. Sci. Am.*, vol. 5, no. 2, pp. 101–111, 1999.

[13] A. Obermair, E. Kucera, K. Mayerhofer, P. Speiser, M. Seifert, K. Czerwenka, A. Kaider, S. Leodolter, C. Kainz, and R. Zeillinger, "Vascular endothelial growth factor (VEGF) in human breast cancer: Correlation with disease-free survival," *Int. J. Cancer*, vol. 74, no. 4, pp. 455–458, 1997.

[14] B. Linderholm, B. Tavelin, K. Grankvist, and R. Henriksson, "Vascular endothelial growth factor is of high prognostic value in node-negative breast carcinoma," *J. Clin. Oncol.*, vol. 16, no. 9, pp. 3121–3128, 1998.

[15] N. Weidner, "Tumoural vascularity as a prognostic factor in cancer patients: The evidence continues to grow," *J. Pathol.*, vol. 184, no. 2, pp. 119–122, 1998.

[16] P.B. Vermeulen, G. Gasparini, S.B. Fox, M. Toi, L. Martin, P. McCulloch, F. Pezzella, G. Viale, N. Weidner, A.L. Harris, and L.Y. Dirix, "Quantification of angiogenesis in solid human tumors: An international consensus on the methodology and criteria of evaluation," *Eur. J. Cancer*, vol. 32A, no. 14, pp. 2474–2484, 1996.

[17] O.A. Kerckhaert and E.E. Voest, "The prognostic and diagnostic value of circulating angiogenic factors in cancer patients," in *Tumor Angiogenesis and Microcirculation*, E.E. Voest and P. A. D'Amore, Eds. New York: Marcel Dekker, Inc., 2001, pp. 487–500.

[18] B. Endrich and P. Vaupel, "The role of microcirculation in the treatment of malignant tumors: Facts and fiction," in *Blood Perfusion and Microenvironment of Human Tumors*, vol. 3, M. Molls and P. Vaupel, Eds. Berlin: Springer-Verlag, 1998, pp. 19–39.

[19] K. Kaban and R.S. Herbst, "Angiogenesis as a target for cancer therapy," *Hematol. Oncol. Clin. North Am.*, vol. 16, no. 5, pp. 1125–1171, 2002.

[20] Z.M. Bhujwalla, D. Artemov, and J. Glockner, "Tumor angiogenesis, vascularization, and contrast-enhanced magnetic resonance imaging," *Top Magn. Reson. Imaging*, vol. 10, no. 2, pp. 92–103, 1999.

[21] R.J. Gillies, Z.M. Bhujwalla, J. Evelhoch, M. Garwood, M. Neeman, S.P. Robinson, C.H. Sotak, and B. Van Der Sanden, "Applications of magnetic resonance in model systems: Tumor biology and physiology," *Neoplasia*, vol. 2, nos. 1–2, pp. 139–151, 2000.

[22] R. Brasch and K. Turetschek, "MRI characterization of tumors and grading angiogenesis using macromolecular contrast media: Status report," *Eur. J. Radiol.*, vol. 34, no. 3, pp. 148–155, 2000.

[23] R.C. Brasch, K.C. Li, J.E. Husband, M.T. Keogan, M. Neeman, A.R. Padhani, D. Shames, and K. Turetschek, "In vivo monitoring of tumor angiogenesis with MR imaging," *Acad. Radiol.*, vol. 7, no. 10, pp. 812–823, 2000.

[24] R. Weissleder and U. Mahmood, "Molecular imaging," *Radiology*, vol. 219, no. 2, pp. 316–333, 2001.

[25] F.A. Howe, S.P. Robinson, D.J. McIntyre, M. Stubbs, and J.R. Griffiths, "Issues in flow and oxygenation dependent contrast (FLOOD) imaging of tumors," *NMR Biomed.*, vol. 14, nos. 7–8, pp. 497–506, 2001.

[26] P.L. Choyke, A.J. Dwyer, and M.V. Knopp, "Functional tumor imaging with dynamic contrast-enhanced magnetic resonance imaging," *J. Magn. Reson. Imaging*, vol. 17, no. 5, pp. 509–520, 2003.

[27] G.J. Parker and P.S. Tofts, "Pharmacokinetic analysis of neoplasms using contrast-enhanced dynamic magnetic resonance imaging," *Top Magn. Reson. Imaging*, vol. 10, no. 2, pp. 130–142, 1999.

[28] A.R. Padhani, "Dynamic contrast-enhanced MRI in clinical oncology: Current status and future directions," *J. Magn. Reson. Imaging*, vol. 16, no. 4, pp. 407–422, 2002.

[29] H.E. Daldrup, D.M. Shames, W. Husseini, M.F. Wendland, Y. Okuhata, and R.C. Brasch, "Quantification of the extraction fraction for gadopentetate across breast cancer capillaries," *Magn. Reson. Med.*, vol. 40, no. 4, pp. 537–543, 1998.

[30] P.S. Tofts, G. Brix, D.L. Buckley, J.L. Evelhoch, E. Henderson, M.V. Knopp, H.B. Larsson, T.Y. Lee, N.A. Mayr, G.J. Parker, R.E. Port, J. Taylor, and R.M. Weisskoff, "Estimating kinetic parameters from dynamic contrast-enhanced T(1)-weighted MRI of a diffusable tracer: Standardized quantities and symbols," *J. Magn. Reson. Imaging*, vol. 10, no. 3, pp. 223–232, 1999.

[31] E.L. Barbier, L. Lamalle, and M. Decorps, "Methodology of brain perfusion imaging," *J. Magn. Reson. Imaging*, vol. 13, no. 4, pp. 496–520, 2001.

[32] A.G. Sorensen, A.L. Tievsky, L. Ostergaard, R.M. Weisskoff, and B.R. Rosen, "Contrast agents in functional MR imaging," *J. Magn. Reson. Imaging*, vol. 7, no. 1, pp. 47–55, 1997.

[33] K.L. Zierler, "Theory of use of indicators to measure blood flow and extracellular volume and calculation of trans capillary movement of tracers," *Circulation Res.*, vol. 12, pp. 464–471, 1963.

[34] C. Crone, "The permeability of capillaries in various organs as determined by the use of 'indicator diffusion' method," *Acta Physiol. Scand*, vol. 58, pp. 292–305, 1963.

[35] S.S. Kety, "The theory and applications of the exchange of inert gas at the lungs and tissues," *Pharmacol. Rev.*, vol. 3, pp. 1–41, 1951.

[36] C.Z. Simonsen, L. Ostergaard, D.F. Smith, P. Vestergaard-Poulsen, and C. Gyldensted, "Comparison of gradient- and spin-echo imaging: CBF, CBV, and MTT measurements by bolus tracking," *J. Magn. Reson. Imaging*, vol. 12, no. 3, pp. 411–416, 2000.

[37] J. Dennie, J.B. Mandeville, J.L. Boxerman, S.D. Packard, B.R. Rosen, and R.M. Weisskoff, "NMR imaging of changes in vascular morphology due to tumor angiogenesis," *Magn. Reson. Med.*, vol. 40, no. 6, pp. 793–799, 1998.

[38] R. Bruening, C. Berchtenbreiter, N. Holzknecht, M. Essig, R.H. Wu, A. Simmons, A. Heuck, A. Maschek, M. Meusel, S.C. Williams, T. Cox, M.V. Knopp, and M. Reiser, "Effects of three different doses of a bolus injection of gadodiamide: Assessment of regional cerebral blood volume maps in a blinded reader study," *AJNR Amer. J. Neuroradiol.*, vol. 21, no. 9, pp. 1603–1610, 2000.

[39] M. Rausch, K. Scheffler, M. Rudin, and E.W. Radu, "Analysis of input functions from different arterial branches with gamma variate functions and cluster analysis for quantitative blood volume measurements," *Magn. Reson. Imaging*, vol. 18, no. 10, pp. 1235–1243, 2000.

[40] B.R. Rosen, J.W. Belliveau, B.R. Buchbinder, R.C. McKinstry, L.M. Porkka, D.N. Kennedy, M.S. Neuder, C.R. Fisel, H.J. Aronen, K.K. Kwong, et al., "Contrast agents and cerebral hemodynamics," *Magn. Reson. Med.*, vol. 19, no. 2, pp. 285–292, 1991.

[41] L. Ostergaard, A.G. Sorensen, K.K. Kwong, R.M. Weisskoff, C. Gyldensted, and B.R. Rosen, "High resolution measurement of cerebral blood flow using intravascular tracer bolus passages. Part II: Experimental comparison and preliminary results," *Magn. Reson. Med.*, vol. 36, no. 5, pp. 726–736, 1996.

[42] A. Jackson, A. Kassner, X.P. Zhu, and K.L. Li, "Reproducibility of T2* blood volume and vascular tortuosity maps in cerebral gliomas," *J. Magn. Reson. Imaging*, vol. 14, no. 5, pp. 510–516, 2001.

[43] F. Wenz, K. Rempp, G. Brix, M.V. Knopp, F. Guckel, T. Hess, and G. van Kaick, "Age dependency of the regional cerebral blood volume (rCBV) measured with dynamic susceptibility contrast MR imaging (DSC)," *Magn. Reson. Imaging*, vol. 14, no. 2, pp. 157–162, 1996.

[44] F. Wenz, K. Rempp, T. Hess, J. Debus, G. Brix, R. Engenhart, M.V. Knopp, G. van Kaick, and M. Wannenmacher, "Effect of radiation on blood volume in low-grade astrocytomas and normal brain tissue: Quantification with dynamic susceptibility contrast MR imaging," *AJR Amer. J. Roentgenol.*, vol. 166, no. 1, pp. 187–193, 1996.

[45] M.E. Moseley, Z. Vexler, H.S. Asgari, J. Mintorovitch, N. Derugin, S. Rocklage, and J. Kucharczyk, "Comparison of Gd- and Dy-chelates for T2 contrast-enhanced imaging," *Magn. Reson. Med.*, vol. 22, no. 2, pp. 259–264, 1991.

[46] P. Reimer, G. Schuierer, T. Balzer, and P.E. Peters, "Application of a superparamagnetic iron oxide (Resovist) for MR imaging of human cerebral blood volume," *Magn. Reson. Med.*, vol. 34, no. 5, pp. 694–697, 1995.

[47] M.H. Lev, S.F. Kulke, A.G. Sorensen, J.L. Boxerman, T.J. Brady, B.R. Rosen, B.R. Buchbinder, and R.M. Weisskoff, "Contrast-to-noise ratio in functional MRI of relative cerebral blood volume with sprodiamide injection," *J. Magn. Reson. Imaging*, vol. 7, no. 3, pp. 523–527, 1997.

[48] R.L. De La Paz, I.L. Ott, and T. Paola, "Recurrent brain tumor versus radiation necrosis: Comparison of MR relative cerebral blood volume maps and FDG-PET," *Radiology*, vol. 197, p. 169, 1995.

[49] M. Forsting, W. Reith, A. Dorfler, R. von Kummer, W. Hacke, and K. Sartor, "MRI in acute cerebral ischaemia: Perfusion imaging with superparamagnetic iron oxide in a rat model," *Neuroradiology*, vol. 36, no. 1, pp. 23–26, 1994.

[50] A. Bjornerud, L.O. Johansson, and H.K. Ahlstrom, "Renal T(*)(2) perfusion using an iron oxide nanoparticle contrast agent-influence of T(1) relaxation on the first-pass response," *Magn. Reson. Med.*, vol. 47, no. 2, pp. 298–304, 2002.

[51] T. Bjerner, L. Johansson, A. Ericsson, G. Wikstrom, A. Hemmingsson, and

H. Ahlstrom, "First-pass myocardial perfusion MR imaging with outer-volume suppression and the intravascular contrast agent NC100150 injection: Preliminary results in eight patients," *Radiology*, vol. 221, no. 3, pp. 822–826, 2001.
[52] J.A. d'Arcy, D.J. Collins, I.J. Rowland, A.R. Padhani, and M.O. Leach, "Applications of sliding window reconstruction with cartesian sampling for dynamic contrast enhanced MRI," *NMR Biomed.*, vol. 15, no. 2, pp. 174–183, 2002.
[53] S. Cha, S. Lu, G. Johnson, and E.A. Knopp, "Dynamic susceptibility contrast MR imaging: Correlation of signal intensity changes with cerebral blood volume measurements," *J. Magn. Reson. Imaging*, vol. 11, no. 2, pp. 114–119, 2000.
[54] M. Maeda, S. Itoh, H. Kimura, T. Iwasaki, N. Hayashi, K. Yamamoto, Y. Ishii, and T. Kubota, "Tumor vascularity in the brain: Evaluation with dynamic susceptibility-contrast MR imaging," *Radiology*, vol. 189, no. 1, pp. 233–238, 1993.
[55] T. Siegal, R. Rubinstein, T. Tzuk-Shina, and J.M. Gomori, "Utility of relative cerebral blood volume mapping derived from perfusion magnetic resonance imaging in the routine follow up of brain tumors," *J. Neurosurg.*, vol. 86, no. 1, pp. 22–27, 1997.
[56] E.L. Barbier, J.A. den Boer, A.R. Peters, A.R. Rozeboom, J. Sau, and A. Bonmartin, "A model of the dual effect of gadopentetate dimeglumine on dynamic brain MR images," *J. Magn. Reson. Imaging*, vol. 10, no. 3, pp. 242–253, 1999.
[57] T. Hacklander, J.R. Reichenbach, and U. Modder, "Comparison of cerebral blood volume measurements using the T1 and T2* methods in normal human brains and brain tumors," *J. Comput. Assist. Tomogr.*, vol. 21, no. 6, pp. 857–866, 1997.
[58] H.J. Aronen, I.E. Gazit, D.N. Louis, B.R. Buchbinder, F.S. Pardo, R.M. Weisskoff, G.R. Harsh, G.R. Cosgrove, E.F. Halpern, F.H. Hochberg, et al., "Cerebral blood volume maps of gliomas: Comparison with tumor grade and histologic findings," *Radiology*, vol. 191, no. 1, pp. 41–51, 1994.
[59] T. Sugahara, Y. Korogi, Y. Shigematsu, L. Liang, K. Yoshizumi, M. Kitajima, and M. Takahashi, "Value of dynamic susceptibility contrast magnetic resonance imaging in the evaluation of intracranial tumors," *Top Magn. Reson. Imaging*, vol. 10, no. 2, pp. 114–124, 1999.
[60] L. Ostergaard, F.H. Hochberg, J.D. Rabinov, A.G. Sorensen, M. Lev, L. Kim, R.M. Weisskoff, R.G. Gonzalez, C. Gyldensted, and B.R. Rosen, "Early changes measured by magnetic resonance imaging in cerebral blood flow, blood volume, and blood-brain barrier permeability following dexamethasone treatment in patients with brain tumors," *J. Neurosurg.*, vol. 90, no. 2, pp. 300–315, 1999.
[61] A.G. Sorensen, W.A. Copen, L. Ostergaard, F.S. Buonanno, R.G. Gonzalez, G. Rordorf, B.R. Rosen, L.H. Schwamm, R.M. Weisskoff, and W.J. Koroshetz, "Hyperacute stroke: Simultaneous measurement of relative cerebral blood volume, relative cerebral blood flow, and mean tissue transit time," *Radiology*, vol. 210, no. 2, pp. 519–527, 1999.
[62] A.P. Pathak, K.M. Schmainda, B.D. Ward, J.R. Linderman, K.J. Rebro, and A.S. Greene, "MR-derived cerebral blood volume maps: Issues regarding histological validation and assessment of tumor angiogenesis," *Magn. Reson. Med.*, vol. 46, no. 4, pp. 735–747, 2001.
[63] S. Cha, G. Johnson, Y.Z. Wadghiri, O. Jin, J. Babb, D. Zagzag, and D.H. Turnbull, "Dynamic, contrast-enhanced perfusion MRI in mouse gliomas: Correlation with histopathology," *Magn. Reson. Med.*, vol. 49, no. 5, pp. 848–855, 2003.
[64] T. Sugahara, Y. Korogi, M. Kochi, I. Ikushima, T. Hirai, T. Okuda, Y. Shigematsu, L. Liang, Y. Ge, Y. Ushio, and M. Takahashi, "Correlation of MR imaging-determined cerebral blood volume maps with histologic and angiographic determination of vascularity of gliomas," *AJR Amer. J. Roentgenol.*, vol. 171, no. 6, pp. 1479–1486, 1998.
[65] H.J. Aronen, J. Glass, F.S. Pardo, J.W. Belliveau, M.L. Gruber, B.R. Buchbinder, I.E. Gazit, R.M. Linggood, A.J. Fischman, B.R. Rosen, et al., "Echo-planar MR cerebral blood volume mapping of gliomas. Clinical utility," *Acta. Radiol.*, vol. 36, no. 5, pp. 520–528, 1995.
[66] E.A. Knopp, S. Cha, G. Johnson, A. Mazumdar, J.G. Golfinos, D. Zagzag, D.C. Miller, P.J. Kelly, and Kricheff, II, "Glial neoplasms: Dynamic contrast-enhanced T2*-weighted MR imaging," *Radiology*, vol. 211, no. 3, pp. 791–798, 1999.
[67] L.J. Bagley, R.I. Grossman, K.D. Judy, M. Curtis, L.A. Loevner, M. Polansky, and J. Detre, "Gliomas: Correlation of magnetic susceptibility artifact with histologic grade," *Radiology*, vol. 202, no. 2, pp. 511–516, 1997.
[68] T. Ichikawa, H. Haradome, J. Hachiya, T. Nitatori, and T. Araki, "Characterization of hepatic lesions by perfusion-weighted MR imaging with an echoplanar sequence," *AJR Amer. J. Roentgenol.*, vol. 170, no. 4, pp. 1029–1034, 1998.
[69] C.K. Kuhl, H. Bieling, J. Gieseke, T. Ebel, P. Mielcarek, F. Far, P. Folkers, A. Elevelt, and H.H. Schild, "Breast neoplasms: T2* susceptibility-contrast, first-pass perfusion MR imaging," *Radiology*, vol. 202, no. 1, pp. 87–95, 1997.
[70] K.A. Kvistad, S. Lundgren, H.E. Fjosne, E. Smenes, H.B. Smethurst, and O. Haraldseth, "Differentiating benign and malignant breast lesions with T2*-weighted first pass perfusion imaging," *Acta. Radiol.*, vol. 40, no. 1, pp. 45–51, 1999.
[71] K.L. Weind, C.F. Maier, B.K. Rutt, and M. Moussa, "Invasive carcinomas and fibroadenomas of the breast: Comparison of microvessel distributions—implications for imaging modalities," *Radiology*, vol. 208, no. 2, pp. 477–483, 1998.
[72] M.W. Ah-See, A. Makris, N.J. Taylor, M. Harrison, P. Richman, R.J. Burcombe, J.J. Stirling, H.J. Cladd, M.O. Leach, and A.R. Padhani, "Multi-functional magnetic resonance imaging predicts for clinico-pathological response to neoadjuvant chemotherapy in primary breast cancer," presented at *26th Annu. San Antonio Breast Cancer Symp.*, San Antonio, 2003.
[73] H.B. Larsson, M. Stubgaard, J.L. Frederiksen, M. Jensen, O. Henriksen, and O.B. Paulson, "Quantitation of blood-brain barrier defect by magnetic resonance imaging and gadolinium-DTPA in patients with multiple sclerosis and brain tumors," *Magn. Reson. Med.*, vol. 16, no. 1, pp. 117–131, 1990.
[74] P. Gowland, P. Mansfield, P. Bullock, M. Stehling, B. Worthington, and J. Firth, "Dynamic studies of gadolinium uptake in brain tumors using inversion-recovery echo-planar imaging," *Magn. Reson. Med.*, vol. 26, no. 2, pp. 241–258, 1992.
[75] G.J. Parker, J. Suckling, S.F. Tanner, A.R. Padhani, P.B. Revell, J.E. Husband, and M.O. Leach, "Probing tumor microvascularity by measurement, analysis and display of contrast agent uptake kinetics," *J. Magn. Reson. Imaging.*, vol. 7, no. 1, pp. 564–574, 1997.
[76] M.Y. Su, J.C. Jao, and O. Nalcioglu, "Measurement of vascular volume fraction and blood-tissue permeability constants with a pharmacokinetic model: Studies in rat muscle tumors with dynamic Gd-DTPA enhanced MRI," *Magn. Reson. Med.*, vol. 32, no. 6, pp. 714–724, 1994.
[77] M.Y. Su, Y.C. Cheung, J.P. Fruehauf, H.Yu,O. Nalcioglu, E. Mechetner, A. Kyshtoobayeva, S.C. Chen, S. Hsueh, C.E. McLaren, and Y.L. Wan, "Correlation of dynamic contrast enhancement MRI parameters with microvessel density and VEGF for assessment of angiogenesis in breast cancer," *J. Magn. Reson. Imaging*, vol. 18, no. 4, pp. 467–477, 2003.
[78] C.K. Kuhl, P. Mielcareck, S. Klaschik, C. Leutner, E. Wardelmann, J. Gieseke, and H.H. Schild, "Dynamic breast MR imaging: Are signal intensity time course data useful for differential diagnosis of enhancing lesions?," *Radiology*, vol. 211, no. 1, pp. 101–110, 1999.
[79] B.L. Daniel, Y.F. Yen, G.H. Glover, D.M. Ikeda, R.L. Birdwell, A.M. Sawyer-Glover, J.W. Black, S.K. Plevritis, S.S. Jeffrey, and R.J. Herfkens, "Breast disease: Dynamic spiral MR imaging," *Radiology*, vol. 209, no. 2, pp. 499–509, 1998.
[80] F.W. Flickinger, J.D. Allison, R.M. Sherry, and J.C. Wright, "Differentiation of benign from malignant breast masses by time-intensity evaluation of contrast enhanced MRI," *Magn. Reson. Imaging*, vol. 11, no. 5, pp. 617–620, 1993.
[81] W.A. Kaiser and E. Zeitler, "MR imaging of the breast: Fast imaging sequences with and without Gd-DTPA. Preliminary observations," *Radiology*, vol. 170, no. 3, pp. 681–686, 1989.
[82] I.S. Gribbestad, G. Nilsen, H.E. Fjosne, S. Kvinnsland, O.A. Haugen, and P.A. Rinck, "Comparative signal intensity measurements in dynamic gadolinium-enhanced MR mammography," *J. Magn. Reson. Imaging*, vol. 4, no. 3, pp. 477–480, 1994.
[83] J.L. Evelhoch, "Key factors in the acquisition of contrast kinetic data for oncology," *J. Magn. Reson. Imaging*, vol. 10, no. 3, pp. 254–259, 1999.
[84] S. Walker, A.S. Dzik-Jurasz, J.A. D'arcy, M.O. Leach, and D.J. Collins, "Evaluation of area under curve [Gd] data derived from DCE-MRI time series in brain tumors," presented at *Proc. Int. Soc. Magn. Reson. Med.*, Toronto, 2003.
[85] G.J. Parker, I. Baustert, S.F. Tanner, and M.O. Leach, "Improving image quality and T(1) measurements using saturation recovery turboFLASH with an approximate K-space normalisation filter," *Magn. Reson. Imaging*, vol. 18, no. 2, pp. 157–167, 2000.
[86] P.S. Tofts and A.G. Kermode, "Measurement of the blood-brain barrier permeability and leakage space using dynamic MR imaging. 1. Fundamental concepts," *Magn. Reson. Med.*, vol. 17, no. 2, pp. 357–367, 1991.
[87] H.B. Larsson and P.S. Tofts, "Measurement of blood-brain barrier permeability using dynamic Gd-DTPA scanning—a comparison of methods," *Magn. Reson. Med.*, vol. 24, no. 1, pp. 174–176, 1992.
[88] H.J. Weinmann, M. Laniado, and W. Mutzel, "Pharmacokinetics of GdDTPA/dimeglumine after intravenous injection into healthy volunteers," *Physiol. Chem. Phys. Med. NMR*, vol. 16, no. 2, pp. 167–172, 1984.
[89] P.S. Tofts, "Modeling tracer kinetics in dynamic Gd-DTPA MR imaging" *J. Magn. Reson. Imaging*, vol. 7, no. 1, pp. 91–101, 1997.
[90] B.M. Dale, J.A. Jesberger, J.S. Lewin, C.M. Hillenbrand, and J.L. Duerk, "Determining and optimizing the precision of quantitative measurements of perfusion from dynamic contrast enhanced MRI," *J. Magn. Reson. Imaging*, vol. 18, no. 5, pp. 575–584, 2003.
[91] F. Kiessling, M. Krix, M. Heilmann, S. Vosseler, M. Lichy, C. Fink, N. Farhan, K. Kleinschmidt, L. Schad, N.E. Fusenig, and S. Delorme, "Comparing dynamic parameters of tumor vascularization in nude mice revealed by magnetic resonance imaging and contrast-enhanced intermittent power Doppler sonography," *Invest. Radiol.*, vol. 38, no. 8, pp. 516–524, 2003.
[92] D. Cosgrove, R. Eckersley, M. Blomley, and C. Harvey, "Quantification of blood flow," *Eur. Radiol.*, vol. 11, no. 8, pp. 1338–1344, 2001.
[93] M.W. Ah-See, A.R. Padhani, N.J. Taylor, F.M. Daley, S.M. Bentzen, R.J. Burcombe, M. Harrison, J.J. Stirling, M.O. Leach, and A. Makris, "Evaluation of VEGF expression within breast cancer biopsies & tumor microvasculature assessment by multi-functional dynamic contrast-enhanced MRI," presented at *The 4th Eur. Breast Cancer Conf. (EBCC-4)*, Hamburg, Germany, 2004.
[94] R.J. Maxwell, J. Wilson, V.E. Prise, B. Vojnovic, G.J. Rustin, M.A. Lodge, and G.M. Tozer, "Evaluation of the anti-vascular effects of combretastatin in rodent tumors by dynamic contrast enhanced MRI," *NMR Biomed.*, vol. 15, no. 2, pp. 89–98, 2002.
[95] P.S. Tofts, B. Berkowitz, and M.D. Schnall, "Quantitative analysis of dynamic Gd-DTPA enhancement in breast tumors using a permeability model," *Magn. Reson. Med.*, vol. 33, no. 4, pp. 564–568, 1995.
[96] C.S. Landis, X. Li, F.W. Telang, J.A. Coderre, P.L. Micca, W.D. Rooney, L.L. Latour, G. Vetek, I. Palyka, and C.S. Springer, Jr., "Determination of the MRI contrast agent concentration time course in vivo following bolus injection: Effect

of equilibrium transcytolemmal water exchange," *Magn. Reson. Med.*, vol. 44, no. 4, pp. 563–574, 2000.
[97] D.L. Buckley, "Transcytolemmal water exchange and its affect on the determination of contrast agent concentration in vivo," *Magn. Reson. Med.*, vol. 47, no. 2, pp. 420–421, 2002.
[98] D.L. Buckley, "Uncertainty in the analysis of tracer kinetics using dynamic contrast-enhanced T(1)-weighted MRI," *Magn. Reson. Med.*, vol. 47, no. 3, pp. 601–606, 2002.
[99] P.C. Stomper, J.S. Winston, S. Herman, D.L. Klippenstein, M.A. Arredondo, and L.E. Blumenson, "Angiogenesis and dynamic MR imaging gadolinium enhancement of malignant and benign breast lesions," *Breast Cancer Res. Treat.*, vol. 45, no. 1, pp. 39–46, 1997.
[100] H. Hawighorst, P.G. Knapstein, W. Weikel, M.V. Knopp, I. Zuna, A. Knof, G. Brix, U. Schaeffer, C. Wilkens, S.O. Schoenberg, M. Essig, P. Vaupel, and G. van Kaick, "Angiogenesis of uterine cervical carcinoma: Characterization by pharmacokinetic magnetic resonance parameters and histological microvessel density with correlation to lymphatic involvement," *Cancer Res.*, vol. 57, no. 21, pp. 4777–4786, 1997.
[101] O. Tynninen, H.J. Aronen, M. Ruhala, A. Paetau, K. Von Boguslawski, O. Salonen, J. Jaaskelainen, and T. Paavonen, "MRI enhancement and microvascular density in gliomas. Correlation with tumor cell proliferation," *Invest. Radiol.*, vol. 34, no. 6, pp. 427–434, 1999.
[102] D.L. Buckley, P.J. Drew, S. Mussurakis, J.R. Monson, and A. Horsman, "Microvessel density of invasive breast cancer assessed by dynamic Gd-DTPA enhanced MRI," *J. Magn. Reson. Imaging*, vol. 7, no. 3, pp. 461–464, 1997.
[103] H.P. Schlemmer, J. Merkle, R. Grobholz, T. Jaeger, M.S. Michel, A. Werner, J. Rabe, and G. Van Kaick, "Can preoperative contrast-enhanced dynamic MR imaging for prostate cancer predict microvessel density in prostatectomy specimens?," *Eur. Radiol.*, vol. 14, no. 2, pp. 309–317, 2003.
[104] A. Carriero, *R.* Ambrossini, P.A. Mattei, D. Angelucci, and L. Bonomo, "Magnetic resonance of the breast: Correlation between enhancement patterns and microvessel density in malignant tumors," *J. Exp. Clin. Cancer. Res.*, vol. 21, no. 3, pp. 83–87, 2002.
[105] C.A. Hulka, W.B. Edmister, B.L. Smith, L. Tan, D.C. Sgroi, T. Campbell, D.B. Kopans, and R.M. Weisskoff, "Dynamic echo-planar imaging of the breast: Experience in diagnosing breast carcinoma and correlation with tumor angiogenesis," *Radiology*, vol. 205, no. 3, pp. 837–842, 1997.
[106] R.A. Cooper, B.M. Carrington, J.A. Loncaster, S.M. Todd, S.E. Davidson, J.P. Logue, A.D. Luthra, A.P. Jones, I. Stratford, R.D. Hunter, and C.M. West, "Tumor oxygenation levels correlate with dynamic contrast-enhanced magnetic resonance imaging parameters in carcinoma of the cervix," *Radiother. Oncol.*, vol. 57, no. 1, pp. 53–59, 2000.
[107] M.V. Knopp, E. Weiss, H.P. Sinn, J. Mattern, H. Junkermann, J. Radeleff, A. Magener, G. Brix, S. Delorme, I. Zuna, and G. van Kaick, "Pathophysiologic basis of contrast enhancement in breast tumors," *J. Magn. Reson. Imaging*, vol. 10, no. 3, pp. 260–266, 1999.
[108] Z.M. Bhujwalla, D. Artemov, *K.* Natarajan, E. Ackerstaff, and M. Solaiyappan, "Vascular differences detected by MRI for metastatic versus non-metastatic breast and prostate cancer xenografts," *Neoplasia*, vol. 3, no. 2, pp. 143–153, 2001.
[109] C.D. Pham, T.P. Roberts, N. van Bruggen, O. Melnyk, J. Mann, N. Ferrara, R.L. Cohen, and R.C. Brasch, "Magnetic resonance imaging detects suppression of tumor vascular permeability after administration of antibody to vascular endothelial growth factor," *Cancer Invest.*, vol. 16, no. 4, pp. 225–230, 1998.
[110] A. Gossmann, T.H. Helbich, N. Kuriyama, S. Ostrowitzki, T.P. Roberts, D.M. Shames, N. van Bruggen, M.F. Wendland, M.A. Israel, and R.C. Brasch, "Dynamic contrast-enhanced magnetic resonance imaging as a surrogate marker of tumor response to anti-angiogenic therapy in a xenograft model of glioblastoma multiforme," *J. Magn. Reson. Imaging*, vol. 15, no. 3, pp. 233–240, 2002.
[111] D. Checkley, J.J. Tessier, J. Kendrew, J.C. Waterton, and S.R. Wedge, "Use of dynamic contrast-enhanced MRI to evaluate acute treatment with ZD6474, a VEGF signalling inhibitor, in PC-3 prostate tumors," *Br. J. Cancer*, vol. 89, no. 10, no. 3, pp. 1889–1895, 2003.
[112] K. Turetschek, A. Preda, E. Floyd, D.M. Shames, V. Novikov, T.P. Roberts, J.M. Wood, Y. Fu, W.O. Carter, and R.C. Brasch, "MRI monitoring of tumor response following angiogenesis inhibition in an experimental human breast cancer model," *Eur. J. Nucl. Med. Mol. Imaging*, vol. 30, no. 3, pp. 448–455, 2003.
[113] B. Morgan, A.L. Thomas, J. Drevs, J. Hennig, M. Buchert, A. Jivan, M.A. Horsfield, K. Mross, H.A. Ball, L. Lee, W. Mietlowski, S. Fuxius, C. Unger, K. O'Byrne, *A.* Henry, G.R. Cherryman, D. Laurent, M. Dugan, D. Marme, and W.P. Steward, "Dynamic contrast-enhanced magnetic resonance imaging as a biomarker for the pharmacological response of PTK787/ZK 222584, an inhibitor of the vascular endothelial growth factor receptor tyrosine kinases, in patients with advanced colorectal cancer and liver metastases: Results from two phase I studies," *J. Clin. Oncol.*, vol. 21, no. 21, pp. 3955–3964, 2003.
[114] G.C. Jayson, J. Zweit, A. Jackson, C. Mulatero, P. Julyan, M. Ranson, L. Broughton, J. Wagstaff, L. Hakannson, G. Groenewegen, J. Bailey, N. Smith, D. Hastings, J. Lawrance, H. Haroon, T. Ward, *A.T.* McGown, M. Tang, D. Levitt, S. Marreaud, F.F. Lehmann, M. Herold, and H. Zwierzina, "Molecular imaging and biological evaluation of HuMV833 anti-VEGF antibody: Implications for trial design of antiangiogenic antibodies," *Natl. Cancer. Inst.*, vol. 94, no. 19, pp. 1484–1493, 2002.
[115] W.K.A. Yung, H. Friedman, C. Conrad, D. Reardon, J. Provenzale, E. Jackson, N. Leeds, H. Serajuddin, D. Laurent, and D. Reitsma, "A phase I trial of single-agent PTK 787/ZK 222584 (PTK/ZK), an oral VEGFR tyrosine kinase inhibitor, in patients with recurrent glioblastoma multiforme," presented at *ASCO*, Chicago, 2003.
[116] R. Matsubayashi, Y. Matsuo, G. Edakuni, T. Satoh, O. Tokunaga, and S. Kudo, "Breast masses with peripheral rim enhancement on dynamic contrast-enhanced MR images: Correlation of MR findings with histologic features and expression of growth factors," *Radiology*, vol. 217, no. 3, pp. 841–848, 2000.
[117] Y. Yamashita, T. Baba, Y. Baba, R. Nishimura, S. Ikeda, M. Takahashi, H. Ohtake, and H. Okamura, "Dynamic contrast-enhanced MR imaging of uterine cervical cancer: Pharmacokinetic analysis with histopathologic correlation and its importance in predicting the outcome of radiation therapy," *Radiology*, vol. 216, no. 3, pp. 803–809, 2000.
[118] H. Lyng, A.O. Vorren, K. Sundfor, I. Taksdal, H.H. Lien, O. Kaalhus, and E.K. Rofstad, "Assessment of tumor oxygenation in human cervical carcinoma by use of dynamic Gd-DTPA-enhanced MR imaging," *J. Magn. Reson. Imaging*., vol. 14, no. 6, pp. 750–756, 2001.
[119] H. Konouchi, J. Asaumi, Y. Yanagi, H. Shigehara, M. Hisatomi, H. Matsuzaki, and K. Kishi, "Evaluation of tumor proliferation using dynamic contrast enhanced-MRI of oral cavity and oropharyngeal squamous cell carcinoma," *Oral. Oncol.*, vol. 39, no. 3, pp. 290–295, 2003.
[120] H.J. van der Woude, K.L. Verstraete, P.C. Hogendoorn, A.H. Taminiau, J. Hermans, and J.L. Bloem, "Musculoskeletal tumors: Does fast dynamic contrast-enhanced subtraction MR imaging contribute to the characterization?," *Radiology*, vol. 208, no. 3, pp. 821–828, 1998.
[121] L. Ludemann, B. Hamm, and C. Zimmer, "Pharmacokinetic analysis of glioma compartments with dynamic Gd-DTPA-enhanced magnetic resonance imaging," *Magn. Reson. Imaging*, vol. 18, pp. 1201–1214, 2000.
[122] H.C. Roberts, T.P. Roberts, A.W. Bollen, S. Ley, R.C. Brasch, and W.P. Dillon, "Correlation of microvascular permeability derived from dynamic contrast-enhanced MR imaging with histologic grade and tumor labeling index: A study in human brain tumors," *Acad. Radiol.*, vol. 8, no. 5, pp. 384–391, 2001.
[123] H.C. Roberts, T.P. Roberts, R.C. Brasch, and W.P. Dillon, "Quantitative measurement of microvascular permeability in human brain tumors achieved using dynamic contrast-enhanced MR imaging: Correlation with histologic grade," *Amer. J. Neuroradiol.*, vol. 21, no. 5, pp. 891–899, 2000.
[124] P.F. Liu, G.P. Krestin, R.A. Huch, S.C. Gohde, R.F. Caduff, and J.F. Debatin, "MRI of the uterus, uterine cervix, and vagina: Diagnostic performance of dynamic contrast-enhanced fast multiplanar gradient-echo imaging in comparison with fast spin-echo T2-weighted pulse imaging," *Eur. Radiol.*, vol. 8, no. 8, pp. 1433–1440, 1998.
[125] J.O. Barentsz, G.J. Jager, P.B. van Vierzen, J.A. Witjes, S.P. Strijk, H. Peters, N. Karssemeijer, and S.H. Ruijs, "Staging urinary bladder cancer after transurethral biopsy: Value of fast dynamic contrast-enhanced MR imaging," *Radiology*, vol. 201, no. 1, pp. 185–193, 1996.
[126] G.J. Jager, E.T. Ruijter, C.A. van de Kaa, J.J. de la Rosette, G.O. Oosterhof, J.R. Thornbury, S.H. Ruijs, and J.O. Barentsz, "Dynamic TurboFLASH subtraction technique for contrast-enhanced MR imaging of the prostate: Correlation with histopathologic results," *Radiology*, vol. 203, no. 3, pp. 645–652, 1997.
[127] R.A. Huch Boni, J.A. Boner, U.M. Lutolf, F. Trinkler, D.M. Pestalozzi, and G.P. Krestin, "Contrast-enhanced endorectal coil MRI in local staging of prostate carcinoma," *J. Comput. Assist. Tomogr.*, vol. 19, no. 2, pp. 232–237, 1995.
[128] H. Hawighorst, W. Weikel, P.G. Knapstein, M.V. Knopp, I. Zuna, S.O. Schonberg, P. Vaupel, and G. van Kaick, "Angiogenic activity of cervical carcinoma: Assessment by functional magnetic resonance imaging-based parameters and a histomorphological approach in correlation with disease outcome," *Clin. Cancer Res.*, vol. 4, no. 10, pp. 2305–2312, 1998.
[129] R. Gilles, J.M. Guinebretiere, L.G. Shapeero, A. Lesnik, G. Contesso, D. Sarrazin, J. Masselot, and D. Vanel, "Assessment of breast cancer recurrence with contrast-enhanced subtraction MR imaging: Preliminary results in 26 patients," *Radiology*, vol. 188, no. 2, pp. 473–478, 1993.
[130] R.W. Kerslake, J.N. Fox, P.J. Carleton, M.J. Imrie, A.M. Cook, S.J. Bowsley, and A. Horsman, "Dynamic contrast-enhanced and fat suppressed magnetic resonance imaging in suspected recurrent carcinoma of the breast: Preliminary experience," *Br. J. Radiol.*, vol. 67, no. 804, pp. 1158–1168, 1994.
[131] S. Mussurakis, D.L. Buckley, S.J. Bowsley, P.J. Carleton, J.N. Fox, L.W. Turnbull, and A. Horsman, "Dynamic contrast-enhanced magnetic resonance imaging of the breast combined with pharmacokinetic analysis of gadolinium-DTPA uptake in the diagnosis of local recurrence of early stage breast carcinoma," *Invest Radiol.*, vol. 30, no. 11, pp. 650–662, 1995.
[132] K. Kinkel, A.A. Tardivon, P. Soyer, A. Spatz, P. Lasser, P. Rougier, and D. Vanel, "Dynamic contrast-enhanced subtraction versus T2-weighted spin-echo MR imaging in the follow-up of colorectal neoplasm: A prospective study of 41 patients," *Radiology*, vol. 200, no. 2, pp. 453–458, 1996.
[133] J.M. Hawnaur, X.P. Zhu, and C.E. Hutchinson, "Quantitative dynamic contrast enhanced MRI of recurrent pelvic masses in patients treated for cancer," *Br. J. Radiol.*, vol. 71, no. 851, pp. 1136–1142, 1998.
[134] T.H. Dao, A. Rahmouni, F. Campana, M. Laurent, B. Asselain, and A. Fourquet, "Tumor recurrence versus fibrosis in the irradiated breast: Differentiation with dynamic gadolinium-enhanced MR imaging," *Radiology*, vol. 187, no. 3, pp. 751–755, 1993.
[135] S.H. Heywang-Kobrunner, A. Schlegel, R. Beck, T. Wendt, W. Kellner, B. Lommatzsch, M. Untch, and W.B. Nathrath, "Contrast-enhanced MRI of the breast after limited surgery and radiation therapy," *J. Comput. Assist. Tomogr.*, vol. 17, no. 6, pp. 891–900, 1993.
[136] L. Blomqvist, P. Fransson, and T. Hindmarsh, "The pelvis after surgery and radio-chemotherapy for rectal cancer studied with Gd-DTPA-enhanced fast

dynamic MR imaging," *Eur. Radiol.*, vol. 8, no. 5, pp. 781–787, 1998.
[137] J.O. Barentsz, O. Berger-Hartog, J.A. Witjes, C. Hulsbergen-van der Kaa, G.O. Oosterhof, J.A. VanderLaak, H. Kondacki, and S.H. Ruijs, "Evaluation of chemotherapy in advanced urinary bladder cancer with fast dynamic contrast-enhanced MR imaging," *Radiology*, vol. 207, no. 3, pp. 791–797, 1998.
[138] W.E. Reddick, J.S. Taylor, and B.D. Fletcher, "Dynamic MR imaging (DEMRI) of microcirculation in bone sarcoma," *J. Magn. Reson. Imaging*, vol. 10, no. 3, pp. 277–285, 1999.
[139] H.J. van der Woude, J.L. Bloem, K.L. Verstraete, A.H. Taminiau, M.A. Nooy, and P.C. Hogendoorn, "Osteosarcoma and Ewing's sarcoma after neoadjuvant chemotherapy: Value of dynamic MR imaging in detecting viable tumor before surgery," *Amer. J. Roentgenol.*, vol. 165, no. 3, pp. 593–598, 1995.
[140] M.V. Knopp, G. Brix, H.J. Junkermann, and H.P. Sinn, "MR mammography with pharmacokinetic mapping for monitoring of breast cancer treatment during neoadjuvant therapy," *Magn. Reson. Imaging Clin. N. Am.*, vol. 2, no. 4, pp. 633–658, 1994.
[141] A.F. Devries, J. Griebel, C. Kremser, W. Judmaier, T. Gneiting, A. Kreczy, D. Ofner, K.P. Pfeiffer, G. Brix, and P. Lukas, "Tumor microcirculation evaluated by dynamic magnetic resonance imaging predicts therapy outcome for primary rectal carcinoma," *Cancer Res.*, vol. 61, no. 6, pp. 2513–2516, 2001.
[142] A. de Vries, J. Griebel, C. Kremser, W. Judmaier, T. Gneiting, P. Debbage, T. Kremser, K.P. Pfeiffer, W. Buchberger, and P. Lukas, "Monitoring of tumor microcirculation during fractionated radiation therapy in patients with rectal carcinoma: Preliminary results and implications for therapy," *Radiology*, vol. 217, no. 2, pp. 385–391, 2000.
[143] N.A. Mayr, W.T. Yuh, J.C. Arnholt, J.C. Ehrhardt, J.I. Sorosky, V.A. Magnotta, K.S. Berbaum, W. Zhen, A.C. Paulino, L.W. Oberley, A.K. Sood, and J.M. Buatti, "Pixel analysis of MR perfusion imaging in predicting radiation therapy outcome in cervical cancer," *J. Magn. Reson. Imaging*, vol. 12, no. 6, pp. 1027–1033, 2000.
[144] M.L. George, A.S. Dzik-Jurasz, A.R. Padhani, G. Brown, D.M. Tait, S.A. Eccles, and R.I. Swift, "Non-invasive methods of assessing angiogenesis and their value in predicting response to treatment in colorectal cancer," *Br. J. Surg.*, vol. 88, no. 12, pp. 1628–1636, 2001.
[145] A.R. Padhani, A.D. MacVicar, C.J. Gapinski, D.P. Dearnaley, G.J. Parker, J. Suckling, M.O. Leach, and J.E. Husband, "Effects of androgen deprivation on prostatic morphology and vascular permeability evaluated with MR imaging," *Radiology*, vol. 218, no. 2, pp. 365–374, 2001.
[146] P.R. Burn, J.M. McCall, R.J. Chinn, A. Vashisht, J.R. Smith, and J.C. Healy, "Uterine fibroleiomyoma: MR imaging appearances before and after embolization of uterine arteries," *Radiology*, vol. 214, no. 3, no. 1, pp. 729–734, 2000.
[147] R.C. Jha, S.M. Ascher, I. Imaoka, and J.B. Spies, "Symptomatic fibroleiomyomata: MR imaging of the uterus before and after uterine arterial embolization," *Radiology*, vol. 217, pp. 228–235, 2000.
[148] W. Li, D.P. Brophy, Q. Chen, R.R. Edelman, and P.V. Prasad, "Semiquantitative assessment of uterine perfusion using first pass dynamic contrast-enhanced MR imaging for patients treated with uterine fibroid embolization," *J. Magn. Reson. Imaging*, vol. 12, no. 6, pp. 1004–1008, 2000.
[149] S.M. Galbraith, R.J. Maxwell, M.A. Lodge, G.M. Tozer, J. Wilson, N.J. Taylor, J.J. Stirling, L. Sena, A.R. Padhani, and G.J. Rustin, "Combretastatin A4 phosphate has tumor antivascular activity in rat and man as demonstrated by dynamic magnetic resonance imaging," *J. Clin. Oncol.*, vol. 21, no. 15, pp. 2831–2842, 2003.
[150] S.M. Galbraith, G.J. Rustin, M.A. Lodge, N.J. Taylor, J.J. Stirling, M. Jameson, P. Thompson, D. Hough, L. Gumbrell, and A.R. Padhani, "Effects of 5,6-dimethylxanthenone-4-acetic acid on human tumor microcirculation assessed by dynamic contrast-enhanced magnetic resonance imaging," *J. Clin. Oncol.*, vol. 20, no. 18, pp. 3826–3840, 2002.
[151] S.M. Galbraith, R.J. Maxwell, M.A. Lodge, G.M. Tozer, J. Wilson, N.J. Taylor, J.J. Stirling, L. Sena, A.R. Padhani, and G.J. Rustin, "Combretastatin A4 phosphate has tumor antivascular activity in rat and man as demonstrated by dynamic magnetic resonance imaging," *J. Clin. Oncol*, 2003.
[152] D. Vincensini, V. Dedieu, J.P. Renou, P. Otal, and F. Joffre, "Measurements of extracellular volume fraction and capillary permeability in tissues using dynamic spin-lattice relaxometry: Studies in rabbit muscles," *Magn. Reson. Imaging*, vol. 21, no. 2, pp. 85–93, 2003.
[153] C. Boetes, J.O. Barentsz, R.D. Mus, R.F. van der Sluis, L.J. van Erning, J.H. Hendriks, R. Holland, and S.H. Ruys, "MR characterization of suspicious breast lesions with a gadolinium-enhanced TurboFLASH subtraction technique," *Radiology*, vol. 193, no. 3, pp. 777–781, 1994.
[154] U. Hoffmann, G. Brix, M.V. Knopp, T. Hess, and W.J. Lorenz, "Pharmacokinetic mapping of the breast: A new method for dynamic MR mammography," *Magn. Reson. Med.*, vol. 33, no. 4, pp. 506–514, 1995.
[155] J.A. den Boer, R.K. Hoenderop, J. Smink, G. Dornseiffen, P.W. Koch, J.H. Mulder, C.H. Slump, E.D. Volker, and R.A. de Vos, "Pharmacokinetic analysis of Gd-DTPA enhancement in dynamic three-dimensional MRI of breast lesions," *J. Magn. Reson. Imaging*, vol. 7, no. 4, pp. 702–715, 1997.
[156] H. Degani, V. Gusis, D. Weinstein, *S.* Fields, and S. Strano, "Mapping pathophysiological features of breast tumors by MRI at high spatial resolution," *Nat. Med.*, vol. 3, no. 7, pp. 780–782, 1997.
[157] J. Evelhoch, T. Brown, T. Chenevert, L. Clake, B. Daniel, H. Degani, N. Hylton, M. Knopp, J.A. Koutcher, T.Y. Lee, N. Mayr, D.C. Sullivan, J. Taylor, P.S. Tofts, and R.M. Weisskoff, "Consensus recommendation for acquisition of dynamic contrast-enhanced MRI data in oncology," presented at *Proc. Int. Soc. Magn. Reson. Med.*, Denver, Colarado, 2000, pp. 1439.
[158] J. Brown, D. Buckley, A. Coulthard, A.K. Dixon, J.M. Dixon, D.F. Easton, R.A. Eeles, D.G. Evans, F.G. Gilbert, M. Graves, C. Hayes, J.P. Jenkins, A.P. Jones, S.F. Keevil, M.O. Leach, G.P. Liney, S.M. Moss, A.R. Padhani, G.J. Parker, L.J. Pointon, B.A. Ponder, T.W. Redpath, J.P. Sloane, L.W. Turnbull, L.G. Walker, and R.M. Warren, "Magnetic resonance imaging screening in women at genetic risk of breast cancer: Imaging and analysis protocol for the UK multicentre study. UK MRI Breast Screening Study Advisory Group," *Magn. Reson. Imaging*, vol. 18, no. 7, pp. 765–776, 2000.
[159] G. Brix, W. Semmler, R. Port, L.R. Schad, G. Layer, and W.J. Lorenz, "Pharmacokinetic parameters in CNS Gd-DTPA enhanced MR imaging," *J. Comput. Assist. Tomogr.*, vol. 15, no. 4, pp. 621–628, 1991.
[160] E. Henderson, B.K. Rutt, and T.Y. Lee, "Temporal sampling requirements for the tracer kinetics modeling of breast disease," *Magn. Reson. Imaging*, vol. 16, no. 9, pp. 1057–1073, 1998.
[161] P.S. Tofts and B.A. Berkowitz, "Measurement of capillary permeability from the Gd enhancement curve: A comparison of bolus and constant infusion injection methods," *Magn. Reson. Imaging*, vol. 12, no. 1, pp. 81–91, 1994.
[162] R.E. Port, M.V. Knopp, U. Hoffmann, S. Milker-Zabel, and G. Brix, "Multicompartment analysis of gadolinium chelate kinetics: Blood-tissue exchange in mammary tumors as monitored by dynamic MR imaging," *J. Magn. Reson. Imaging*, vol. 10, no. 3, pp. 233–241, 1999.
[163] L. Ludemann, B. Hamm, and C. Zimmer, "Pharmacokinetic analysis of glioma compartments with dynamic Gd-DTPA-enhanced magnetic resonance imaging," *Magn. Reson. Imaging*, vol. 18, no. 10, pp. 1201–1214, 2000.
[164] T.P. Roberts, "Physiologic measurements by contrast-enhanced MR imaging: Expectations and limitations," *J. Magn. Reson. Imaging*, vol. 7, no. 1, pp. 82–90, 1997.
[165] A.N. Shetty, K.G. Bis, M. Kirsch, J. Weintraub, and G. Laub, "Contrast-enhanced breath-hold three-dimensional magnetic resonance angiography in the evaluation of renal arteries: Optimization of technique and pitfalls," *J. Magn. Reson. Imaging*, vol. 12, no. 6, pp. 912–923, 2000.
[166] N.J. Taylor, K.J. Lankester, J.J. Stirling, G.J. Rustin, J.A. d'Arcy, M.O. Leach, and A.R. Padhani, "Application of navigator techniques to breath-hold DCE-MRI studies of the liver," presented at *Proc. Int. Soc. Magn. Reson. Med.*, *11th Scientific Meeting*, Toronto, 2003, pp. 1306.
[167] M.D. Noseworthy, M.S. Sussman, M. Haider, and S. Baruchel, "Dynamic contrast enhanced liver MRI using a motion tracking algorithm," presented at *Proc. Int. Soc. Magn. Reson. Med.,* Glasgow, Scotland, 2001, pp. 2240.
[168] C. Tanner, J.A. Schnabel, A. Degenhard, A. Castellano Smith, C. Hayes, M.O. Leach, D.R. Hose, D.L. Hill, and D.J. Hawkes, "Validation of volume preserving non rigid registration: Application to contrast enhanced MR mammography," presented at *Proc. MICCAI'02,* pp. 307–314, 2002.
[169] M.O. Leach, K.M. Brindle, J.L. Evelhoch, J.R. Griffiths, M. Horseman, A. Jackson, I. Judson, M.V. Knopp, R.J. Maxwell, D.J. McIntyre, A.R. Padhani, P. Price, R. Rathbone, G. Rustin, P.S. Tofts, D.J. Tozer, W. Vennart, J. Waterton, P. Williams, and P. Workman, "Assessment of anti-angiogenic and anti-vascular therapeutics using magnetic resonance imaging: Recommendations for appropriate methodology for clinical trials," presented at *Amer. Assoc. Cancer Res.*, Washington, D.C., pp. 504, 2003.
[170] M. Rijpkema, J.H. Kaanders, F.B. Joosten, A.J. van der Kogel, and A. Heerschap, "Method for quantitative mapping of dynamic MRI contrast agent uptake in human tumors," *J. Magn. Reson. Imaging*, vol. 14, no. 4, pp. 457–463, 2001.
[171] S.M. Galbraith, M.A. Lodge, N.J. Taylor, G.J. Rustin, S. Bentzen, J.J. Stirling, and A.R. Padhani, "Reproducibility of dynamic contrast enhanced MRI in human muscle and tumors—comparison of quantitative and semi-quantitative analysis," *NMR Biomed.*, vol. 15, no. 2, pp. 132–142, 2002.
[172] A.R. Padhani, C. Hayes, S. Landau, and M.O. Leach, "Reproducibility of Quantitative Dynamic MRI of Normal Human Tissues," *NMR Biomed.*, vol. 15, no. 2, pp. 143–154, 2002.
[173] J. Evelhoch, P. LoRusso, Z. Latif, P. Morton, W. Wolf, M. McKinley, J. Waterton, and A. Barge, "Reproducibility of dynamic contrast-enhanced (DCE-MRI) assessment of tumor vascularity," presented at *Amer. Soc. Clin. Oncol. 2001 Annu. Meeting*, San Francisco, CA, p. 399, 2001.
[174] C. Hayes, A.R. Padhani, and M.O. Leach, "Assessing changes in tumor vascular function using dynamic contrast-enhanced magnetic resonance imaging," *NMR Biomed.*, vol. 15, no. 2, pp. 154–163, 2002.
[175] X.P. Zhu, K.L. Li, I.D. Kamaly-Asl, D.R. Checkley, J.J. Tessier, J.C. Waterton, and A. Jackson, "Quantification of endothelial permeability, leakage space, and blood volume in brain tumors using combined T1 and T2* contrast-enhanced dynamic MR imaging," *J. Magn. Reson. Imaging*, vol. 11, no. 6, pp. 575–585, 2000.
[176] J.B. Bassingthwaighte, L.S. Liebovitch, and B.J. West, *Fractal Physiology*. Oxford, U.K.: Oxford Univ. Press, 1994.
[177] C.D. Collins, S. Walker, A.S. Dzik-Jurasz, and M.O. Leach, "Fractral analysis of parametric images derived from dynamic contrast enhanced MRI data in-vivo: Methods for describing dispersion in parametric data," presented at *Proc. Int. Soc. Magn. Reson. Med.*, Toronto, Canada, 2003, p. 1269.